Vol 18 No 2, February 2009
1674-1056/2009/18(02)/0825-20

Chinese Physics B

© 2009 Chin. Phys. Soc.
and IOP Publishing Ltd

Development of the spectrum of gamma-ray burst pulses influenced by the intrinsic spectral evolution and the curvature effect*

Qin Yi-Ping(覃一平)[a)b)]

[a)] *Center for Astrophysics, Guangzhou University, Guangzhou* 510006, *China*

[b)] *Physics Department, Guangxi University, Nanning* 530004, *China*

(Received 17 September 2007; revised manuscript received 7 August 2008)

The spectral evolution of gamma-ray burst pulses assumed to arise from the emission of fireballs is explored. It is found that due to the curvature effect, the integrated flux is well related to peak energy by a power law in the decaying phase of pulses, where the index is about 3, which does not depend on intrinsic emission and the Lorentz factor. The spectra of pulses in the decaying phase are slightly different from each other when different intrinsic spectral evolution patterns are considered, indicating that it is dominated by the curvature effect. In the rising phase, the integrated flux keeps increasing whilst the peak energy remains unchanged when the intrinsic emission bears an unchanged spectrum. Within this phase, the flux decreases with the increase of the peak energy for a hard-to-soft intrinsic spectrum, and for a soft-to-hard-to-soft intrinsic spectrum, the flux generally increases with the increase of the peak energy. An intrinsic soft-to-hard-to-soft spectral evolution within a co-moving pulse would give rise to a pulse-like evolutionary curve for the peak energy.

Keywords: gamma-ray bursts, gamma-rays, relativity
PACC: 9870Q, 9580Q

1. Introduction

Recent Swift observations of early x-ray afterglows of gamma-ray bursts (GRBs) have revealed that the previous interpretation of the GRB afterglow, which was based on the mechanism of external shocks, is unlikely to be the mechanism accounting for these new findings. Instead, the internal shock origin and the so-called 'curvature effect' might be responsible for many of the early x-ray afterglows.[1−8] The curvature effect is a combined effect that includes the delay of time and the shifting of the intrinsic spectrum as well as other relevant factors of an expanding fireball (see Ref.[9] for a detailed explanation). The effect was widely investigated in recent years in both the prompt emission and early x-ray afterglow of GRBs.[4,7−9,10−23]

Early study of the spectral evolution of GRBs revealed that the general evolution of the spectra of these objects was hard-to-soft as shown in Ref.[24] This issue was also frequently investigated in recent years.[11,25−28] It is shown in Ref.[14] that the hardness-intensity correlation could be accounted for by the curvature effect. Authors of Ref.[9] explored the evolutionary curve of the hardness ratio (HRC) of GRB pulses and concluded that the main characteristics of the HRC of some GRB fast rise exponential decay (FRED) pulses accorded with what was predicted by the curvature effect. In addition, they showed that the curvature effect alone could not completely explain the observed HRCs. Instead, a hard-to-soft intrinsic spectral evolution might exist and probably play a role in producing the observed HRCs.

Here in the present paper, we investigate how the intrinsic spectral evolution and the curvature effect combine to produce an observed spectrum arising from a fireball pulse. The remainder of the present paper is organized as follows. In Section 2, we present formulae that can be directly applied to the case of the intrinsic spectral evolution. Spectral evolution within a pulse of fireballs, radiated in the form of a typical intrinsic emission, is investigated in various aspects in Section 3. In Section 4, other forms of intrinsic emission are considered. In Section 5, we direct our attention to various situations of the soft-to-hard-to-soft intrinsic emission. Influence of the Lorentz factor on the spec-

*Project supported by the National Natural Science Foundation of China (Grant Nos 10573005 and 10747001).

tral evolution is investigated in Section 6. Section 7 presents a symbol of the curvature effect shown by the evolutionary curve of the peak energy in the decaying phase of pulses. Conclusions drawn from the present study are given in Section 8.

2. General formulae of flux and count rates for expanding fireballs

Here we present more general formulae than those derived in Refs.[13] and [19] so that they could be directly applied to various cases of the intrinsic spectral evolution pattern. For more general applications, formulae with various variables are provided.

2.1. Formulae in terms of the integral of θ

For a radiation associated with an intrinsic emission independent of direction, the expected flux of a fireball expanding with a constant Lorentz factor is[13]

$$f_\nu(t) = \frac{2\pi}{D^2}\int_{\tilde{\theta}_{\min}}^{\tilde{\theta}_{\max}} I_\nu(t',\nu,\nu_0)R^2(t')\cos\theta\sin\theta \mathrm{d}\theta, \quad (1)$$

where $I_\nu(t',\ \nu,\ \nu_0)$ is the intensity in the observer frame; ν is the observation frequency; ν_0 is the frequency in the rest frame, which is the frequency of emission from differential surface $\mathrm{d}s_\theta$, which gives rise to ν (see expression (9) presented below for the relation between I_ν and ν_0); t is the observation time; D is the distance from the fireball to the observer; θ is the angle of $\mathrm{d}s_\theta$ of the fireball, to the line of sight; t' is the emission time (in the observer frame), called local time, of photons that emit from $\mathrm{d}s_\theta$; $R(t')$ is the radius of the fireball measured at time t'. The integral range of θ, i.e. $\tilde{\theta}_{\min}$ and $\tilde{\theta}_{\max}$, will be determined by the concerned area of the fireball surface as well as the emission ranges of the frequency and the local time. As shown in Refs.[13] and [19], t' is related to t by

$$t' = \frac{t - t_{\mathrm{c}} - \dfrac{D}{c} + \dfrac{R_{\mathrm{c}}}{c}\cos\theta}{1-\beta\cos\theta} + t_{\mathrm{c}}, \quad (2)$$

where t_{c} and R_{c} are constants. Assume that the area of the fireball surface concerned is confined within

$$\theta_{\min} \le \theta \le \theta_{\max}, \quad (3)$$

and the emission time t' is confined within

$$t_{\mathrm{c}} \le t'_{\min} \le t' \le t'_{\max}. \quad (4)$$

Except them we assume that there is no any other constraint to the integral limit of expression (1). According to expressions (3) and (4), one can verify that the lower and the upper integral limits of expression (1) could be determined by

$$\tilde{\theta}_{\min} = \cos^{-1}\min\left\{\cos\theta_{\min}, \frac{t'_{\max} - t + \dfrac{D}{c}}{(t'_{\max} - t_{\mathrm{c}})\beta + \dfrac{R_{\mathrm{c}}}{c}}\right\} \quad (5)$$

and

$$\tilde{\theta}_{\max} = \cos^{-1}\max\left\{\cos\theta_{\max}, \frac{t'_{\min} - t + \dfrac{D}{c}}{(t'_{\min} - t_{\mathrm{c}})\beta + \dfrac{R_{\mathrm{c}}}{c}}\right\}, \quad (6)$$

respectively (for a detailed derivation, one could refer to Refs.[13] and [19]). Applying the relation between the radius of the fireball and the observation time we come to the following form of flux (see Refs.[13] and [19]):

$$f_\nu(t) = \frac{2\pi[(t - t_{\mathrm{c}} - \dfrac{D}{c})\beta c + R_{\mathrm{c}}]^2}{D^2} \times \int_{\tilde{\theta}_{\min}}^{\tilde{\theta}_{\max}} \frac{I_\nu(t',\nu,\nu_0)\cos\theta\sin\theta}{(1-\beta\cos\theta)^2}\mathrm{d}\theta. \quad (7)$$

From expression (2) one finds that for arbitrarily given values of t and θ, local time t' would be uniquely determined. If the value of t' is within the range shown in expression (4), then there will be photons emitted at t' from the small surface area of θ, reaching the observer at t [when θ is within the range indicated in expression (3), this small area would be included in the above integral, otherwise it would not]. Obviously, for a certain value of θ, the range of t depends on the range of t'. Inserting expression (2) into expression (4) and applying expression (3) we obtain

$$\begin{aligned}(1-\beta\cos\theta_{\min})t'_{\min} + (t_{\mathrm{c}}\beta - \frac{R_{\mathrm{c}}}{c})\cos\theta_{\min} + \frac{D}{c} \le t \\ \le (1-\beta\cos\theta_{\max})t'_{\max} + (t_{\mathrm{c}}\beta - \frac{R_{\mathrm{c}}}{c})\cos\theta_{\max} + \frac{D}{c}.\end{aligned} \quad (8)$$

This suggests clearly that observation time t is limited when emission time t' is limited.

Let t_0 be the proper time corresponding to the coordinate time t' and ν_0 be the co-moving frequency corresponding to ν. The latter two are related to each other by the Doppler effect. It is well known that the observer frame intensity $I_\nu(t', \nu, \nu_0)$ is related to the rest frame intensity $I_{0,\nu}(t_0, \nu_0)$ by

$$I_\nu(t', \nu, \nu_0) = \left(\frac{\nu}{\nu_0}\right)^3 I_{0,\nu}(t_0, \nu_0), \tag{9}$$

which could be written as

$$I_\nu(t', \nu, \nu_0) = \frac{I_{0,\nu}(t_0, \nu_0)}{(1 - \beta\cos\theta)^3 \Gamma^3}, \tag{10}$$

when the Doppler effect is used. The flux is now able to be written as

$$f_\nu(t) = \frac{2\pi[(t - t_\mathrm{c} - \dfrac{D}{c})\beta c + R_\mathrm{c}]^2}{D^2\Gamma^3} \times \int_{\tilde{\theta}_{\min}}^{\tilde{\theta}_{\max}} \frac{I_{0,\nu}(t_0, \nu_0)\cos\theta\sin\theta}{(1 - \beta\cos\theta)^5}\mathrm{d}\theta, \tag{11}$$

where $\tilde{\theta}_{\min}$ and $\tilde{\theta}_{\max}$ are determined by expressions (5) and (6), respectively, ν_0 and ν are related to each other by the Doppler effect, and t is confined by expression (8).

As t_0 and t' represent the same moment, according to the theory of special relativity, they are related by $t' - t_\mathrm{c} = \Gamma(t_0 - t_{0,\mathrm{c}})$, where $t_{0,\mathrm{c}}$ is a constant (here we assign $t' = t_\mathrm{c}$ when $t_0 = t_{0,\mathrm{c}}$). Take $t' = t'_{\min}|_{t_0 = t_{0,\min}}$ and $t' = t'_{\max}|_{t_0 = t_{0,\max}}$, then we will obtain $t'_{\min} = \Gamma(t_{0,\min} - t_{0,\mathrm{c}}) + t_\mathrm{c}$, and $t'_{\max} = \Gamma(t_{0,\max} - t_{0,\mathrm{c}}) + t_\mathrm{c}$. Then the constraint of expression (4) is identical to

$$t_{0,\mathrm{c}} \le t_{0,\min} \le t_0 \le t_{0,\max}. \tag{12}$$

We then obtain from expressions (5) and (6) that

$$\tilde{\theta}_{\min} = \cos^{-1}\min\left\{\cos\theta_{\min}, \frac{(t_{0,\max} - t_{0,\mathrm{c}})\Gamma + \dfrac{D}{c} - (t - t_\mathrm{c})}{(t_{0,\max} - t_{0,\mathrm{c}})\Gamma\beta + \dfrac{R_\mathrm{c}}{c}}\right\}, \tag{13}$$

and

$$\tilde{\theta}_{\max} = \cos^{-1}\max\left\{\cos\theta_{\max}, \frac{(t_{0,\min} - t_{0,\mathrm{c}})\Gamma + \dfrac{D}{c} - (t - t_\mathrm{c})}{(t_{0,\min} - t_{0,\mathrm{c}})\Gamma\beta + \dfrac{R_\mathrm{c}}{c}}\right\}. \tag{14}$$

In addition, from expression (2) and $t' - t_\mathrm{c} = \Gamma(t_0 - t_{0,\mathrm{c}})$ we obtain

$$t_0 = \frac{t - t_\mathrm{c} - \dfrac{D}{c} + \dfrac{R_\mathrm{c}}{c}\cos\theta}{(1 - \beta\cos\theta)\Gamma} + t_{0,\mathrm{c}} \tag{15}$$

and from $t'_{\min} = \Gamma(t_{0,\min} - t_{0,\mathrm{c}}) + t_\mathrm{c}$, $t'_{\max} = \Gamma(t_{0,\max} - t_{0,\mathrm{c}}) + t_\mathrm{c}$, and expression (8) we acquire

$$\begin{aligned}&(1 - \beta\cos\theta_{\min})[(t_{0,\min} - t_{0,\mathrm{c}})\Gamma + t_\mathrm{c}] + \left(t_\mathrm{c}\beta - \frac{R_\mathrm{c}}{c}\right)\cos\theta_{\min} + \frac{D}{c} \le t \\ &\le (1 - \beta\cos\theta_{\max})[(t_{0,\max} - t_{0,\mathrm{c}})\Gamma + t_\mathrm{c}] + \left(t_\mathrm{c}\beta - \frac{R_\mathrm{c}}{c}\right)\cos\theta_{\max} + \frac{D}{c}.\end{aligned} \tag{16}$$

When calculating the flux from expression (11), we need to convert variable t_0 into θ via expression (15) and convert ν_0 into θ according to the Doppler effect $\nu_0 = (1 - \beta\cos\theta)\Gamma\nu$.

Light curves of GRBs are always presented in terms of count rates within an energy range. The count rate within an energy channel $[\nu_1,\ \nu_2]$ is determined by

$$\frac{\mathrm{d}n(t)}{\mathrm{d}t} = \int_{\nu_1}^{\nu_2} \frac{f_\nu(t)}{h\nu}\mathrm{d}\nu. \tag{17}$$

Inserting expression (11) leads to

$$\frac{\mathrm{d}n(t)}{\mathrm{d}t} = \frac{2\pi[(t-t_{\rm c}-\frac{D}{c})\beta c + R_{\rm c}]^2}{D^2\Gamma^3 h} \times \int_{\tilde{\theta}_{\rm min}}^{\tilde{\theta}_{\rm max}} \left[\int_{\nu_1}^{\nu_2} \frac{I_{0,\nu}(t_0,\nu_0)}{\nu}\mathrm{d}\nu\right] \times \frac{\cos\theta\sin\theta}{(1-\beta\cos\theta)^5}\mathrm{d}\theta. \quad (18)$$

In the case where θ could be treated as a constant, from $\nu_0 = (1-\beta\cos\theta)\Gamma\nu$ one has $\frac{\mathrm{d}\nu}{\nu}|_{\theta=\rm const} = \frac{\mathrm{d}\nu_0}{\nu_0}$. Replacing variable ν with ν_0 we obtain from Eq.(18) that

$$\frac{\mathrm{d}n(t)}{\mathrm{d}t} = \frac{2\pi[(t-t_{\rm c}-\frac{D}{c})\beta c + R_{\rm c}]^2}{D^2\Gamma^3 h} \times \int_{\tilde{\theta}_{\rm min}}^{\tilde{\theta}_{\rm max}} \left[\int_{\nu_{0,1}}^{\nu_{0,2}} \frac{I_{0,\nu}(t_0,\nu_0)}{\nu_0}\mathrm{d}\nu_0\right] \times \frac{\cos\theta\sin\theta}{(1-\beta\cos\theta)^5}\mathrm{d}\theta, \quad (19)$$

where $\nu_{0,1} = (1-\beta\cos\theta)\Gamma\nu_1$ and $\nu_{0,2} = (1-\beta\cos\theta)\Gamma\nu_2$.

2.2. Formulae in terms of the integral of $\cos\theta$

In terms of the integral of $\cos\theta$, the forms of the above formulae become simpler. Let

$$\mu \equiv \cos\theta, \quad (20)$$

$$\mu_{\rm max} \equiv \cos\tilde{\theta}_{\rm min} = \min\left\{\cos\theta_{\rm min}, \frac{(t_{0,\rm max}-t_{0,\rm c})\Gamma + \frac{D}{c} - (t-t_{\rm c})}{(t_{0,\rm max}-t_{0,\rm c})\Gamma\beta + \frac{R_{\rm c}}{c}}\right\}, \quad (21)$$

and

$$\mu_{\rm min} \equiv \cos\tilde{\theta}_{\rm max} = \max\left\{\cos\theta_{\rm max}, \frac{(t_{0,\rm min}-t_{0,\rm c})\Gamma + \frac{D}{c} - (t-t_{\rm c})}{(t_{0,\rm min}-t_{0,\rm c})\Gamma\beta + \frac{R_{\rm c}}{c}}\right\}, \quad (22)$$

where expressions (13) and (14) have been applied.

The flux now can be calculated from

$$f_\nu(t) = \frac{2\pi[(t-t_{\rm c}-\frac{D}{c})\beta c + R_{\rm c}]^2}{D^2\Gamma^3} \times \int_{\mu_{\rm min}}^{\mu_{\rm max}} \frac{I_{0,\nu}(t_0,\nu_0)\mu}{(1-\beta\mu)^5}\mathrm{d}\mu, \quad (23)$$

where t_0 and μ are related by

$$t_0 = \frac{t-t_{\rm c}-\frac{D}{c}+\frac{R_{\rm c}}{c}\mu}{(1-\beta\mu)\Gamma} + t_{0,\rm c} \quad (24)$$

and ν_0 and μ are related by $\nu_0 = (1-\beta\mu)\Gamma\nu$.

The count rate is now determined by

$$\frac{\mathrm{d}n(t)}{\mathrm{d}t} = \frac{2\pi[(t-t_{\rm c}-\frac{D}{c})\beta c + R_{\rm c}]^2}{D^2\Gamma^3 h} \times \int_{\mu_{\rm min}}^{\mu_{\rm max}} \left[\int_{\nu_{0,1}}^{\nu_{0,2}} \frac{I_{0,\nu}(t_0,\nu_0)}{\nu_0}\mathrm{d}\nu_0\right] \times \frac{\mu}{(1-\beta\mu)^5}\mathrm{d}\mu, \quad (25)$$

where $\nu_{0,1} = (1-\beta\mu)\Gamma\nu_1$ and $\nu_{0,2} = (1-\beta\mu)\Gamma\nu_2$.

2.3. Formulae in terms of the integral of the proper emission time

Since the rest frame intensity $I_{0,\nu}(t_0,\nu_0)$ is always provided in the form of the function of the proper emission time t_0, it is more convenient to compute the flux or the count rate from formulae in terms of the integral of t_0.

From expression (24) we obtain

$$\mu = \frac{(t_0-t_{0,\rm c})\Gamma + \frac{D}{c} - (t-t_{\rm c})}{\frac{R_{\rm c}}{c} + (t_0-t_{0,\rm c})\Gamma\beta}, \quad (26)$$

and from $\nu_0 = (1-\beta\mu)\Gamma\nu$ we find

$$\nu_0 = \frac{\frac{R_{\rm c}}{c} - \left[\frac{D}{c} - (t-t_{\rm c})\right]\beta}{\frac{R_{\rm c}}{c} + (t_0-t_{0,\rm c})\Gamma\beta}\Gamma\nu. \quad (27)$$

According to expressions (26) and (27) one can check that inequality $\dfrac{\mathrm{d}t_0}{\mathrm{d}\mu} > 0$.

Replacing μ with t_0, we obtain the following form of formula for calculating the flux:

$$f_\nu(t) = \frac{2\pi c^2 \int_{\tilde{t}_{0,\min}}^{\tilde{t}_{0,\max}} I_{0,\nu}(t_0,\nu_0)\left[(t_0-t_{0,\mathrm{c}})\Gamma + \dfrac{D}{c} - (t-t_{\mathrm{c}})\right]\left[\dfrac{R_{\mathrm{c}}}{c} + (t_0-t_{0,\mathrm{c}})\Gamma\beta\right]^2 \mathrm{d}t_0}{D^2\Gamma^2\left\{\dfrac{R_{\mathrm{c}}}{c} - \left[\dfrac{D}{c} - (t-t_{\mathrm{c}})\right]\beta\right\}^2}, \tag{28}$$

where $\tilde{t}_{0,\min}$ and $\tilde{t}_{0,\max}$ are determined by

$$\tilde{t}_{0,\min} = \max\left\{t_{0,\min}, \frac{t - t_{\mathrm{c}} - \dfrac{D}{c} + \dfrac{R_{\mathrm{c}}}{c}\cos\theta_{\max}}{(1-\beta\cos\theta_{\max})\Gamma} + t_{0,\mathrm{c}}\right\}, \tag{29}$$

and

$$\tilde{t}_{0,\max} = \min\left\{t_{0,\max}, \frac{t - t_{\mathrm{c}} - \dfrac{D}{c} + \dfrac{R_{\mathrm{c}}}{c}\cos\theta_{\min}}{(1-\beta\cos\theta_{\min})\Gamma} + t_{0,\mathrm{c}}\right\}, \tag{30}$$

respectively, and ν_0 and t_0 are related by expression (27).

The count rate is now written in the form

$$\frac{\mathrm{d}n(t)}{\mathrm{d}t} = \frac{2\pi c^2 \int_{\tilde{t}_{0,\min}}^{\tilde{t}_{0,\max}} \left[\int_{\nu_1}^{\nu_2} I_{0,\nu}(t_0,\nu_0)\dfrac{\mathrm{d}\nu}{\nu}\right]\left[(t_0-t_{0,\mathrm{c}})\Gamma + \dfrac{D}{c} - (t-t_{\mathrm{c}})\right]\left[\dfrac{R_{\mathrm{c}}}{c} + (t_0-t_{0,\mathrm{c}})\Gamma\beta\right]^2 \mathrm{d}t_0}{D^2\Gamma^2 h\left\{\dfrac{R_{\mathrm{c}}}{c} - \left[\dfrac{D}{c} - (t-t_{\mathrm{c}})\right]\beta\right\}^2}. \tag{31}$$

According to expression (27), in the case where t and t_0 could be treated as constants we obtain $\dfrac{\mathrm{d}\nu}{\nu}|_{t_0=\mathrm{const},t=\mathrm{const}} = \dfrac{\mathrm{d}\nu_0}{\nu_0}$. Replacing variable ν with ν_0 we can have from Eq.(31) that

$$\frac{\mathrm{d}n(t)}{\mathrm{d}t} = \frac{2\pi c^2 \int_{\tilde{t}_{0,\min}}^{\tilde{t}_{0,\max}} \left[\int_{\nu_{0,1}}^{\nu_{0,2}} \dfrac{I_{0,\nu}(t_0,\nu_0)}{\nu_0}\mathrm{d}\nu_0\right]\left[(t_0-t_{0,\mathrm{c}})\Gamma + \dfrac{D}{c} - (t-t_{\mathrm{c}})\right]\left[\dfrac{R_{\mathrm{c}}}{c} + (t_0-t_{0,\mathrm{c}})\Gamma\beta\right]^2 \mathrm{d}t_0}{D^2\Gamma^2 h\left\{\dfrac{R_{\mathrm{c}}}{c} - \left[\dfrac{D}{c} - (t-t_{\mathrm{c}})\right]\beta\right\}^2}, \tag{32}$$

where $\nu_{0,1} = \left[\dfrac{R_{\mathrm{c}}}{c} - \left(\dfrac{D}{c} - t + t_{\mathrm{c}}\right)\beta\right]\Gamma\nu_1 / \left[\dfrac{R_{\mathrm{c}}}{c} + (t_0 - t_{0,\mathrm{c}})\Gamma\beta\right]$,
and $\nu_{0,2} = \left[\dfrac{R_{\mathrm{c}}}{c} - \left(\dfrac{D}{c} - t + t_{\mathrm{c}}\right)\beta\right]\Gamma\nu_2 / \left[\dfrac{R_{\mathrm{c}}}{c} + (t_0 - t_{0,\mathrm{c}})\Gamma\beta\right]$.

2.4. Formulae in terms of the integral of relative timescales

Assign[19]

$$\begin{aligned}
\tau' &\equiv \frac{t' - t_{\mathrm{c}}}{R_{\mathrm{c}}/c},\\
\tau'_{\min} &\equiv \frac{t'_{\min} - t_{\mathrm{c}}}{R_{\mathrm{c}}/c},\\
\tau'_{\max} &\equiv \frac{t'_{\max} - t_{\mathrm{c}}}{R_{\mathrm{c}}/c},
\end{aligned} \tag{33}$$

$$\begin{aligned}
\tau_0 &\equiv \frac{t_0 - t_{0,\mathrm{c}}}{R_{\mathrm{c}}/c},\\
\tau_{0,\min} &\equiv \frac{t_{0,\min} - t_{0,\mathrm{c}}}{R_{\mathrm{c}}/c},\\
\tau_{0,\max} &\equiv \frac{t_{0,\max} - t_{0,\mathrm{c}}}{R_{\mathrm{c}}/c},
\end{aligned} \tag{34}$$

and

$$\tau \equiv \frac{t - t_{\mathrm{c}} - D/c + R_{\mathrm{c}}/c}{R_{\mathrm{c}}/c}, \tag{35}$$

then one will find that

$$\nu_0 = \frac{1-\beta+\beta\tau}{1+\beta\Gamma\tau_0}\Gamma\nu, \tag{36}$$

$$\tau' = \frac{\tau-(1-\cos\theta)}{1-\beta\cos\theta}, \tag{37}$$

$$0 \le \tau'_{\min} \le \tau' \le \tau'_{\max}, \tag{38}$$

and

$$1-\cos\theta_{\min}+(1-\beta\cos\theta_{\min})\tau'_{\min} \le \tau \le 1 - \cos\theta_{\max}+(1-\beta\cos\theta_{\max})\tau'_{\max}, \tag{39}$$

which is the range of τ within which the radiation defined in the ranges indicated by expressions (3) and (4) is observable. In addition, one has $\tau_{0,\min} = \tau'_{\min}/\Gamma$, $\tau_{0,\max} = \tau'_{\max}/\Gamma$, and

$$1-\cos\theta_{\min}+(1-\beta\cos\theta_{\min})\Gamma\tau_{0,\min} \le \tau \le 1 - \cos\theta_{\max}+(1-\beta\cos\theta_{\max})\Gamma\tau_{0,\max}. \tag{40}$$

Let

$$\tilde{I}_{0,\nu}(\tau_0,\nu_0) \equiv I_{0,\nu}[t_0(\tau_0),\nu_0], \tag{41}$$

then we will obtain from expression (28) that

$$f_\nu(\tau) = \frac{2\pi R_{\rm c}^2 \int_{\tilde{\tau}_{0,\min}}^{\tilde{\tau}_{0,\max}} \tilde{I}_{0,\nu}(\tau_0,\nu_0)(1-\tau+\tau_0\Gamma)(1+\Gamma\beta\tau_0)^2{\rm d}\tau_0}{D^2\Gamma^2(1-\beta+\beta\tau)^2}, \tag{42}$$

where ν_0 is related to τ and ν by expression (36),

$$\tilde{\tau}_{0,\min} = \frac{\tilde{t}_{0,\min}-t_{0,\rm c}}{R_{\rm c}/c} = \max\left\{\tau_{0,\min}, \frac{\tau-1+\cos\theta_{\max}}{(1-\beta\cos\theta_{\max})\Gamma}\right\} \tag{43}$$

and

$$\tilde{\tau}_{0,\max} = \frac{\tilde{t}_{0,\max}-t_{0,\rm c}}{R_{\rm c}/c} = \min\left\{\tau_{0,\max}, \frac{\tau-1+\cos\theta_{\min}}{(1-\beta\cos\theta_{\min})\Gamma}\right\}. \tag{44}$$

Let

$$C(\tau) \equiv \frac{{\rm d}n[t(\tau)]}{{\rm d}\tau}, \tag{45}$$

then we will obtain

$$C(\tau) = \frac{2\pi R_{\rm c}^3 \int_{\tilde{\tau}_{0,\min}}^{\tilde{\tau}_{0,\max}} \left[\int_{\nu_{0,1}}^{\nu_{0,2}} \frac{\tilde{I}_{0,\nu}(\tau_0,\nu_0)}{\nu_0}{\rm d}\nu_0\right](1-\tau+\Gamma\tau_0)(1+\beta\Gamma\tau_0)^2{\rm d}\tau_0}{hcD^2\Gamma^2(1-\beta+\beta\tau)^2}, \tag{46}$$

where $\nu_{0,1} = \frac{(1-\beta+\beta\tau)\Gamma}{1+\beta\Gamma\tau_0}\nu_1$ and $\nu_{0,2} = \frac{(1-\beta+\beta\tau)\Gamma}{1+\beta\Gamma\tau_0}\nu_2$. Note that expressions (42) and (46) hold only when inequality (40) is satisfied. In the range outside the region that is determined by inequality (40), $f_\nu(\tau)$ and $C(\tau)$ will become zero.

Formula (46) shows that the profile of count rate of a fireball source is a function of τ. It is independent of the real time scale t, and also independent of the real size $R_{\rm c}$, of the source. In other words, no matter how big the fireball concerned is and how large the observed timescale concerned is, for the profile of the count rate, only the ratio of the latter to the time scale of the initial radius of the fireball plays a role.

Applying expressions (33) and (34) to $t'-t_{\rm c} = \Gamma(t_0-t_{0,\rm c})$ we obtain $\tau' = \Gamma\tau_0$. Substituting it into expression (37) yields

$$\tau_0 = \frac{\tau-(1-\cos\theta)}{(1-\beta\cos\theta)\Gamma}. \tag{47}$$

Generally, observation time τ is related to the comoving time τ_0 of the surface with the angle relative to the line-of-sight, θ, by

$$\tau = (1-\beta\cos\theta)\Gamma\tau_0 + 1 - \cos\theta. \tag{48}$$

For the same emission time τ_0, photons emitted from surfaces with different angles relative to the line-of-sight would reach the observer at different times. In units of the time scale of the initial radius $R_{\rm c}$, the time delay of photons emitted from θ with respect to that

of photons emitted from $\theta = 0$ is $1 - \cos\theta$. The contraction factor of the emission time is $(1 - \beta\cos\theta)\Gamma$ which differs from surface to surface. Taking $\theta = 0$ we have

$$\tau = (1 - \beta)\Gamma\tau_0, \quad (\theta = 0). \tag{49}$$

This is the relation between the observation time of photons which are emitted from $\theta = 0$ and the corresponding co-moving emission time. The time is contracted by a factor of $(1 - \beta)\Gamma$.

3. Spectral evolution within the period of fireball pulses coming from a typical intrinsic emission form

As revealed in Ref.[9], the observed hardness ratio is seen to be harder at the beginning of some GRB pulses than that the pure curvature effect (when no intrinsic spectral evolution is involved) could predict, and softer at later times of the pulses, thereby causing a so-called 'harder-leading' problem. An economic mechanism was suggested to account for this problem, which is the hard-to-soft evolution pattern of the rest frame spectrum of fireballs (see Ref.[9]). In a more realistic situation, before the hardest spectrum appears, there might be a short period within which the co-moving spectrum undergoes a soft-to-hard phase. This would happen when the inner shell possessed a relatively hard core and surrounding the core are less dense materials. The hardest spectrum will appear when the core strikes the outer shell. Before that the spectrum radiated from the outer shell is softer since the shell is hit by relatively less dense materials and then gains a much smaller acceleration and a smaller speed.

Now we come to investigate the spectral evolution in a simple case where the emission of a co-moving pulse with an exponential rise and exponential decay and with a flexible Comptonized radiation form from the whole fireball surface is observed. For comparison, we consider three co-moving pulses (or rest frame pulses) with their spectra being unchanged, hard-to-soft, and soft-to-hard-to-soft separately during the period concerned. The co-moving pulse with an unchanged spectrum is assumed to be

$$\tilde{I}_{0,\nu}(\tau_0, \nu_0) = I_0\nu_0^{1+\alpha_C}\exp(-\nu_0/\nu_{0,\mathrm{C}}) \begin{cases} \exp\left(-\dfrac{\tau_{0,0} - \tau_0}{\sigma_r}\right), & (\tau_{0,\min} \le \tau_0 \le \tau_{0,0}), \\ \exp\left(-\dfrac{\tau_0 - \tau_{0,0}}{\sigma_d}\right), & (\tau_{0,0} < \tau_0). \end{cases} \tag{50}$$

The co-moving pulse (50) is intrinsically the same as that adopted in Ref.[9]. (Note that $\tau' = \Gamma\tau_0$, or $\tau_0 \propto \tau'$.) The co-moving pulse possessing a hard-to-soft spectral evolution is assumed to be

$$\tilde{I}_{0,\nu}(\tau_0, \nu_0) = I_0\nu_0^{1+\alpha_C}\exp[-(\tau_0/\tau_{0,0})(\nu_0/\nu_{0,\mathrm{C}})] \begin{cases} \exp\left(-\dfrac{\tau_{0,0} - \tau_0}{\sigma_r}\right), & (\tau_{0,\min} \le \tau_0 \le \tau_{0,0}), \\ \exp\left(-\dfrac{\tau_0 - \tau_{0,0}}{\sigma_d}\right), & (\tau_{0,0} < \tau_0), \end{cases} \tag{51}$$

where $\tau_{0,0} \neq 0$. The co-moving pulse with a soft-to-hard-to-soft spectrum is assumed to be

$$\tilde{I}_{0,\nu}(\tau_0, \nu_0) = I_0\nu_0^{1+\alpha_C} \begin{cases} \exp[-(\tau_{0,0}/\tau_0)(\nu_0/\nu_{0,\mathrm{C}})]\exp\left(-\dfrac{\tau_{0,0} - \tau_0}{\sigma_r}\right), & (\tau_{0,\min} < \tau_0 \le \tau_{0,0}), \\ \exp[-(\tau_0/\tau_{0,0})(\nu_0/\nu_{0,\mathrm{C}})]\exp\left(-\dfrac{\tau_0 - \tau_{0,0}}{\sigma_d}\right), & (\tau_{0,0} < \tau_0), \end{cases} \tag{52}$$

where $\tau_0 > 0$ is required (as shown below, this will easily be satisfied). As adopted previously, we assign that $\tau_0 = 10\sigma_r + \tau_{0,\min}$. According to inequality (4), we assign $t' \ge t_c$, which leads to $\tau_{0,\min} \ge 0$. As long as this condition is satisfied, $\tau_{0,\min}$ could be freely chosen. [Note that in the case where $t' \ge t_c$ does not

hold, $\tau_{0,\min}$ is also constrained as $\tau_{0,\min} > -(\beta\Gamma)^{-1}$, when $\beta > 0$ (see Ref.[19]). Without any loss of generality we take $\tau_{0,\min} = 0$. To meet the condition under which the soft-to-hard period is much shorter than the hard-to-soft period in the third co-moving pulse, we take $\sigma_{\rm d} = 2\sigma_{\rm r}$ and this will be applied to all the three co-moving pulses in the following analysis.

Shown in Fig.1 are the spectral evolutions of the three co-moving pulses (50), (51), and (52), where the co-moving times concerned are $\tau_0(1) = \tau_{0,0} - 2\sigma_{\rm r}$, $\tau_0(2) = \tau_{0,0} - \sigma_{\rm r}$, $\tau_0(3) = \tau_{0,0}$, $\tau_0(4) = \tau_{0,0} + \sigma_{\rm d}$, $\tau_0(5) = \tau_{0,0} + 2\sigma_{\rm d}$, $\tau_0(6) = \tau_{0,0} + 4\sigma_{\rm d}$, $\tau_0(7) = \tau_{0,0} + 6\sigma_{\rm d}$, $\tau_0(8) = \tau_{0,0} + 8\sigma_{\rm d}$, $\tau_0(9) = \tau_{0,0} + 10\sigma_{\rm d}$, and $\tau_0(10) = \tau_{0,0} + 12\sigma_{\rm d}$, respectively.

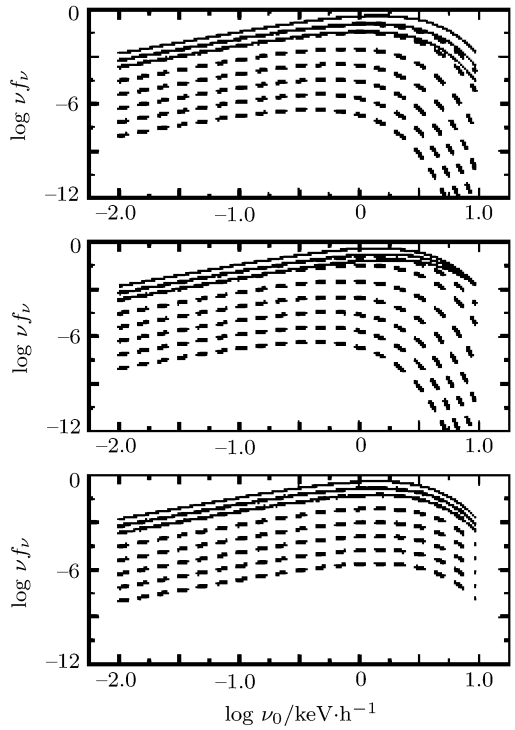


Fig.1. Spectral evolutions of co-moving pulses (50) (the bottom panel), (51) (the mid panel), and (52) (the upper panel) with parameters being $\sigma_{\rm r} = 0.01$, $\sigma_{\rm d} = 2\sigma_{\rm r}$, $\alpha_{0,\rm C} = -0.6$, $\nu_{0,\rm C}$=1 keVh^{-1}, and $I_0 = 1$, and solid lines from the bottom to the top denoting the co-moving times $\tau_0(1)$, $\tau_0(2)$, and $\tau_0(3)$, respectively, and dashed lines from the top to the bottom representing $\tau_0(4)$, $\tau_0(5)$, $\tau_0(6)$, $\tau_0(7)$, $\tau_0(8)$, $\tau_0(9)$, and $\tau_0(10)$, respectively.

Now we come to check how these co-moving pulses give rise to the spectra of fireballs. According to expression (49), the observation times of photons which are emitted from the tip of the fireball (i.e. $\theta = 0$) at the above co-moving times are $\tau(1) = (1-\beta)\Gamma(\tau_{0,0} - 2\sigma_{\rm r})$, $\tau(2) = (1-\beta)\Gamma(\tau_{0,0} - \sigma_{\rm r})$, $\tau(3) = (1-\beta)\Gamma\tau_{0,0}$, $\tau(4) = (1-\beta)\Gamma(\tau_{0,0}+\sigma_{\rm d})$, $\tau(5) = (1-\beta)\Gamma(\tau_{0,0}+2\sigma_{\rm d})$, $\tau(6) = (1-\beta)\Gamma(\tau_{0,0}+4\sigma_{\rm d})$, $\tau(7) = (1-\beta)\Gamma(\tau_{0,0}+6\sigma_{\rm d})$, $\tau(8) = (1-\beta)\Gamma(\tau_{0,0} + 8\sigma_{\rm d})$, $\tau(9) = (1-\beta)\Gamma(\tau_{0,0} + 10\sigma_{\rm d})$, and $\tau(10) = (1-\beta)\Gamma(\tau_{0,0}+12\sigma_{\rm d})$, respectively. Positions of these times in the light curves observed by distant observers are shown in Fig.2, where, expression (46) is employed to calculate the corresponding light curves. The width in the rising part of the co-moving pulses is taken as $\sigma_{\rm r} = 0.0001$ (in the left panels) and $\sigma_{\rm r} = 0.01$ (in the right panels), which correspond to 'narrow' and 'broad' pulses, respectively (see Refs.[17,19]). Solid lines denote the light curves expected in the third channel of burst and transient source experiment (BATSE) (55 keV$\leq E <$110 keV). Dashed lines from the left to the right represent observation times $\tau(1)$, $\tau(2)$, $\tau(3)$, $\tau(4)$, $\tau(5)$, $\tau(6)$, $\tau(7)$, $\tau(8)$, $\tau(9)$, and $\tau(10)$, respectively. Note that equation (21) in Ref.[19] could be applied only to a simple case when the time component and the spectral component of an intrinsic pulse could be separated (see Eq.(10) in Ref.[19]). The advantage of expression (46) is that it could be directly applied to a co-moving radiation which can take any form. For the same reason, expression (42) will be applied to calculate the observed spectrum in the following analysis.

In Fig.2, two typical widths of co-moving pulses are adopted to show how the co-moving width influences the observed spectrum. The words 'narrow' and 'broad' refer to the widths of the profiles of the observed pulses. A 'narrow' pulse comes from a local pulse with a small ratio of its width to the radius of the fireball [or, the ratio of the co-moving pulse width to the product of the radius of the fireball and the Lorentz factor is small; see expression (49)]. A character of this kind of pulse is that the pulse possesses a more steadily decaying phase. Or more precisely, the deviation of its decaying profile from the so-called standard decaying form is mild (for a detailed explanation, see Ref.[17]). Conversely, a 'broad' pulse arises from a local pulse with a large ratio of its width to the radius of the fireball. A character of this kind of pulse is that its decaying profile possesses a reverse S-feature deviation from the standard decaying curve (or the deviation is very obvious).[17]

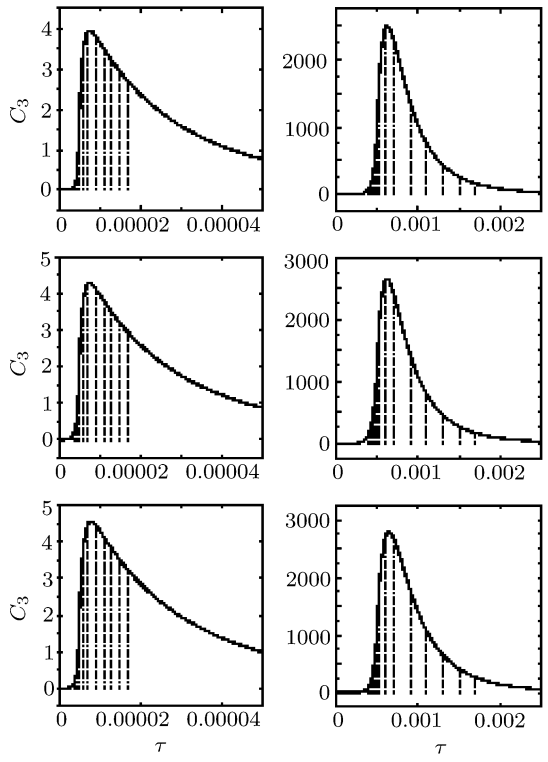


Fig.2. Positions of the observation times corresponding to various co-moving times for photons emitted from the tip of the fireball ($\theta = 0$) marked in the light curves expected by distant observers. The light curves associated with co-moving pulses (50) (bottom panels), (51) (mid panels), and (52) (upper panels) are calculated from expression (46), where $\sigma_{\rm d} = 2\sigma_{\rm r}$, $\alpha_{0,\rm C} = -0.6$, $\nu_{0,\rm C}$=1 keV·h^{-1}, $\Gamma = 100$, and $C_0 \equiv 2\pi R_{\rm c}^3 I_0/hcD^2 = 1$.

3.1. Evolutionary pattern of the overall spectrum

Displayed in Fig.3 are the spectral evolutions within the period of the expected observed pulses of fireballs, which are outcomes of the three co-moving pulses (50), (51) and (52). We use expression (42) to calculate the spectra measured at the observation times $\tau(1)$, $\tau(2)$, $\tau(3)$, $\tau(4)$, $\tau(5)$, $\tau(6)$, $\tau(7)$, $\tau(8)$, $\tau(9)$, and $\tau(10)$. The resulting overall spectra show a general hard-to-soft evolution pattern within the period of the pulses observed. During these observation times, the spectral evolution of 'narrow' pulses is mild (see the left panels in Fig.3), while for 'broad' pulses their spectra develop quite rapidly (see the right panels in Fig.3). In the decaying part of light curves of 'narrow' or 'broad' pulses, the spectral evolution patterns are quite similar to each other for the three co-moving pulses (see dashed lines in Fig. 3). This must be due to the fact that the decaying part of the pulses is dominated by high latitude emission of the fireball, where the curvature effect is important. It is then natural that the spectral evolutions show a similar trend. In the rising part of the light curves of pulses, the scenario is different. The spectral evolution pattern of co-moving pulses obviously influences the way the observed spectrum evolves.

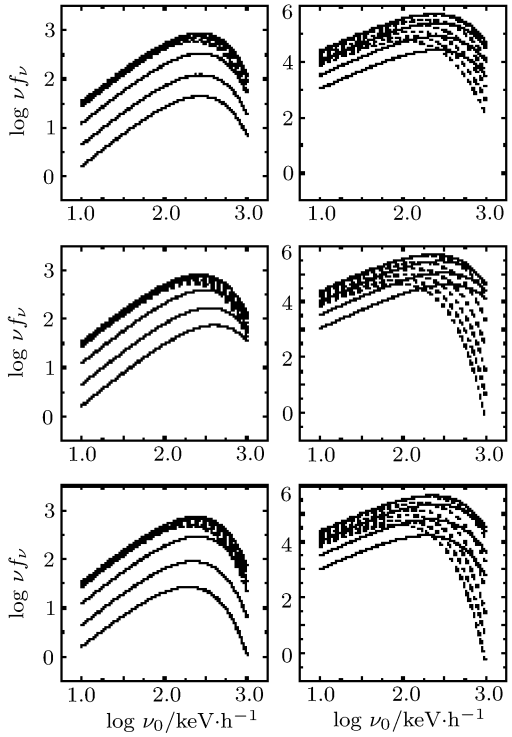


Fig.3. Spectral evolutions of fireball pulses arising from co-moving pulses (50) (bottom panels), (51) (mid panels), and (52) (upper panels). The spectra are calculated from expression (42). Each panel in this plot corresponds to the same panel as that in Fig.2, where the parameters are the same. The only difference is $F_0 \equiv 2\pi R_{\rm c}^2 I_0/D^2 = 1$ that is taken here. In the left panels, solid lines from the bottom to the top denote the spectra measured at observation times $\tau(1)$, $\tau(2)$, $\tau(3)$, $\tau(4)$, and $\tau(5)$, respectively, while dashed lines from the top to the bottom represent the spectra measured at $\tau(6)$, $\tau(7)$, $\tau(8)$, $\tau(9)$, and $\tau(10)$, respectively. In the right panels, solid lines from the bottom to the top represent the spectra measured at $\tau(1)$, $\tau(2)$, $\tau(3)$, and $\tau(4)$, respectively, and dashed lines from the top to the bottom denote the spectra measured at $\tau(5)$, $\tau(6)$, $\tau(7)$, $\tau(8)$, $\tau(9)$, and $\tau(10)$, respectively.

3.2. Evolution of the peak energy of the νf_ν spectrum

There are two quantities capable of describing the hardness of spectra. One is the so-called hardness ratio and the other is the peak energy $E_{\rm p}$ where the peak of νf_ν appears. Evolutions of the two quantities could describe to some extent how the spectrum

evolves. Recently, the hardness ratio curves associated with different situations were discussed.[9] Here, we pay our attention mainly to the evolution of the peak energy within the period of fireball pulses which arise from the three co-moving pulses proposed above.

We employ the following integrated flux (see Section 5) to compare the evolution of $E_{\rm p}$ with light curves:

$$F \equiv \int_{\nu_1}^{\nu_2} f_\nu {\rm d}\nu \tag{53}$$

where ν_1 and ν_2 denote the lower and the upper limits of the energy channel concerned, respectively.

Displayed in Fig.4 are the developments of the peak energy in various cases considered above. The feature of drop-to-rise-to-drop revealed in the hardness ratio curve in Ref.[9] is observed in the peak energy evolutionary curve and it holds only for the unchanged intrinsic spectrum. In the case of intrinsically hard-to-soft spectrum, we observe a continuous hard-to-soft pattern, while in the case of intrinsically soft-to-hard-to-soft spectrum we find a soft-to-hard-to-soft evolution pattern for the observed spectrum. There is a turning point in the $E_{\rm p}(t)$ curve (hereafter EPC). After the turning point, the EPCs associated with the three co-moving pulses show the same trend of softening in the case of 'narrow' pulses. Before the turning point, the observed spectra vary significantly, which is accordant with their intrinsic spectral evolution patterns. This suggests that the spectrum observed before the turning point must mainly be determined by the intrinsic evolution pattern, while after the turning point, it is dominated by the curvature effect. In the 'broad' pulse cases, the softening of the spectra arising from the unchanged intrinsic spectrum co-moving pulses is different from that of the hard-to-soft and soft-to-hard-to-soft intrinsic spectrum co-moving pulses, which leads to a noticeable character discussed below. The sharpness of the turning feature might become an indicator showing a pulse observed to be 'narrow' or 'broad'.

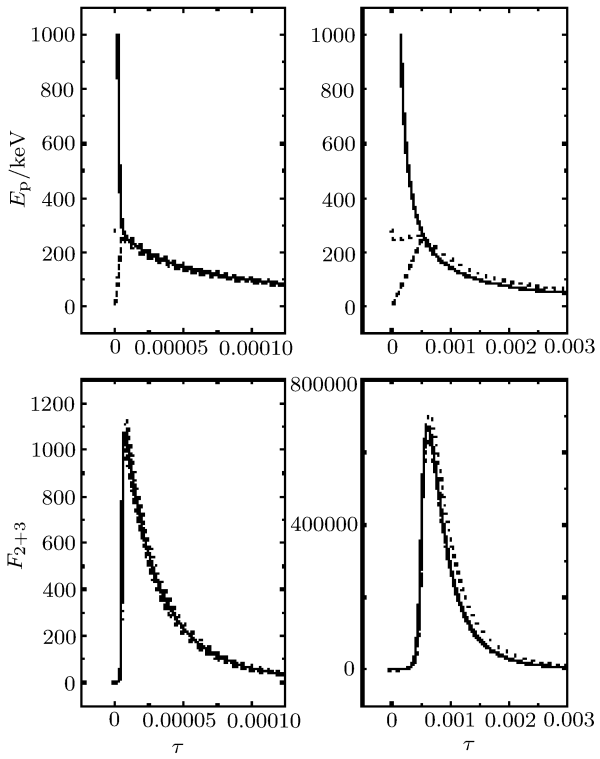


Fig.4. Evolutionary curves of the peak energy (upper panels) of fireball pulses arising from co-moving pulses (50) (dotted lines), (51) (solid lines), and (52) (dashed lines). For comparison, we present in the bottom panels the integrated flux F_{2+3} over the energy range of the second (55 keV$\leq E <$110 keV) and third (110 keV$\leq E <$320 keV) BATSE channels, which are calculated from expressions (42) and (53). Parameters are the same as those in Fig.2. As adopted in Fig.2, the width in the rising part of the co-moving pulses is taken as $\sigma_{\rm r} = 0.0001$ (in the left panels) and $\sigma_{\rm r} = 0.01$ (in the right panels), which correspond to 'narrow' and 'broad' pulses, respectively.

3.3. Comparison of the spectra of emission arising from the tip and from the overall fireball surface

If the fireball moves relativistically towards the observer but it does not expand, one would observe an entirely different evolution pattern of the spectrum within the pulse concerned. Now the question arises whether the spectrum stemming from the expanding fireball is harder or softer than this spectrum. An investigation on this issue might bring us some interesting information. The spectrum of ejecta moving towards the observer must be the same as that emitted from the tip of an expanding fireball surface when the intrinsic spectra and the Lorentz factors are the same.

The spectrum of the emission from the tip of the fireball surface must be merely a blue shift of the intrinsic one. Owing to the contribution of high latitude emissions, a deviation of the observed spectrum of the whole fireball from that of the tip is expected. If the deviation is small within some period of observation time, then one can estimate the form of the intrinsic spectrum from the observed one within this time interval, although the blue shift factor and the amplification factor (or, the boosting factor) remain unknown.

In the following we will investigate how this deviation evolves and what it depends on.

3.3.1. Corresponding overall spectra

The method of comparing the expected tip spectrum with that of the emission from the whole fireball surface is straightforward. One can simply shift the co-moving spectra shown in Fig.1 to high energy ranges where the emission of the tip is expected, and then compare them with those presented in Fig.3. According to the Doppler effect, photons emitted from the tip with frequency ν_0 would be blue shifted to $\nu = \nu_0/\Gamma(1-\beta)$ when they reach the observer. We will use this shift factor, $1/\Gamma(1-\beta)$, to shift the spectra in Fig.1.

Shown in Figs.5, 6 and 7 are the comparisons between spectra of the emission expected to originate from the tip (which is merely the shifting of the intrinsic spectrum) and the emission from the whole fireball surface, for co-moving pulses (50), (51), and (52), respectively. For comparison, we normalize the shifting spectra in Fig.1 by the maxima of the corresponding spectra in Fig.3.

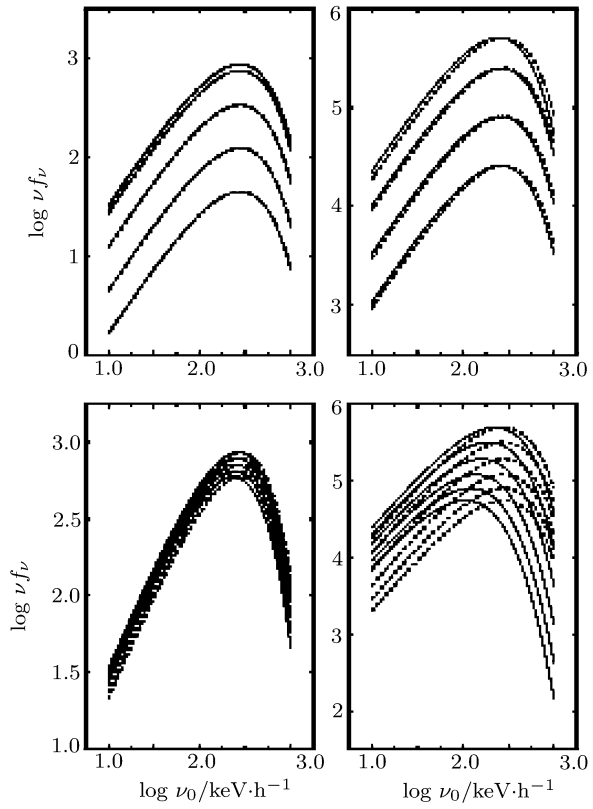


Fig.5. Comparison between spectra expected from the emission of the tip (dashed lines) and the emission from the whole fireball surface (solid lines) in cases of 'narrow' (in the left panels) and 'broad' (in the right panels) pulses arising from the co-moving pulse with an unchanged intrinsic spectrum, i.e. the spectrum of co-moving pulse (50). Solid lines in the left upper and the bottom panels are the solid and the dashed lines in the left bottom panel of Fig.3, respectively. Solid lines in the right upper and the bottom panels are the solid and the dashed lines in the right bottom panel of Fig.3, respectively. Dashed lines denote the shifting lines of the corresponding co-moving spectra presented in the bottom panel of Fig.1, which correspond to the co-moving times (see the caption of Fig.1) when photons emitted at these times from the tip of the fireball surface reach the observer at the times concerned in Fig.3 (see the captions of Figs.2 and 3).

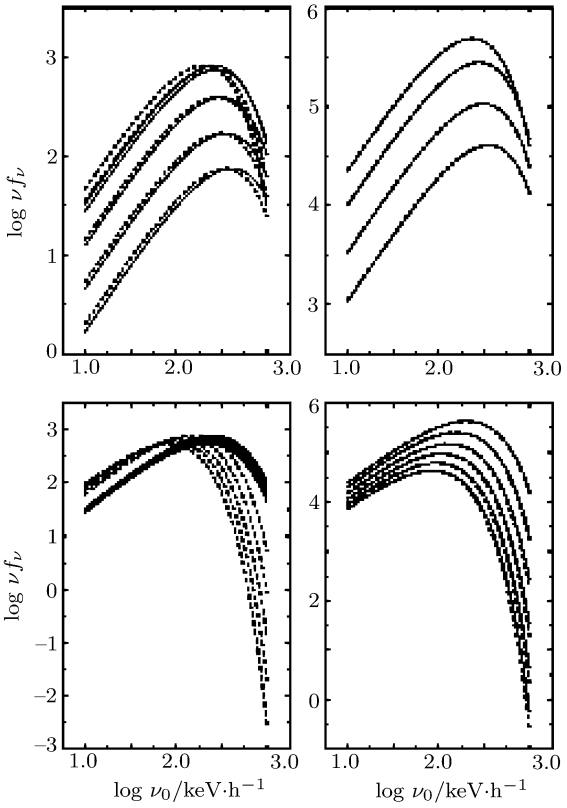


Fig.6. Comparison between spectra of the emission expected to originate from the tip (dashed lines) and the emission from the whole fireball surface (solid lines) in the cases of 'narrow' (in the left panels) and 'broad' (in the right panels) pulses arising from the co-moving pulse with a hard-to-soft intrinsic spectrum, i.e. the spectrum of co-moving pulse (51). Solid lines in the left upper and the left bottom panels are the solid and the dashed lines in the left mid panel of Fig.3, respectively. Solid lines in the right upper and the right bottom panels are the solid and the dashed lines in the right mid panel of Fig.3, respectively. Dashed lines denote the shifting lines of the corresponding co-moving spectra presented in the mid panel of Fig.1. (See Fig.3 for a more detailed explanation.)

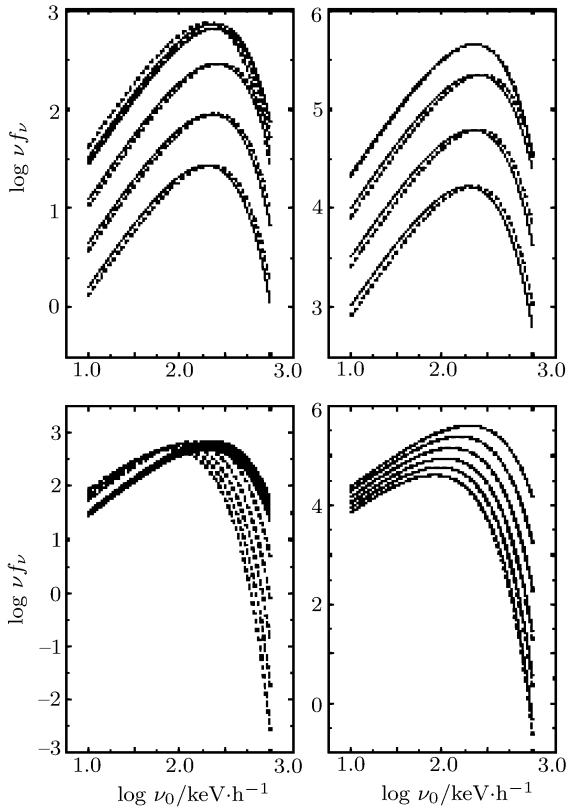


Fig.7. Comparison between spectra of the emission expected to originate from the tip (dashed lines) and the emission from the whole fireball surface (solid lines) in the cases of 'narrow' (in the left panels) and 'broad' (in the right panels) pulses arising from the co-moving pulse with a soft-to-hard-to-soft intrinsic spectrum, i.e. the spectrum of co-moving pulse (52). Solid lines in the left upper and the left bottom panels are the solid and the dashed lines in the left upper panel of Fig.3, respectively. Solid lines in the right upper and the right bottom panels are the solid and the dashed lines in the right upper panel of Fig.3, respectively. Dashed lines denote the shifting lines of the corresponding co-moving spectra presented in the upper panel of Fig. 1. (See Fig.3 for a more detailed explanation.)

In the case of the unchanged intrinsic spectrum, the observed spectrum in the rising part of the light curve for 'narrow' pulses is almost the same as that expected to be emitted from the tip of fireball (see the left upper panel of Fig.5), while it deviates slightly from the latter for 'broad' pulses (see the right upper panel of the figure). In the decaying portion, the observed spectra are obviously softer than that expected to be emitted from the tip of fireball, and the softening is very significant for 'broad' pulses (see the two lower panels of Fig.5). This indicates that if an unchanged spectrum during the rising part of pulses is observed, then the corresponding intrinsic spectrum is likely to be an unchanged one.

When the evolution of the intrinsic spectrum is hard-to-soft, the observed spectrum is also hard-to-soft. In the rising part of the light curve of 'broad' pulses, the spectrum is almost the same as that of the emission expected from the tip of fireball (see the left upper panel of Fig.6), while in the decaying portion of the light curve it deviates slightly from the latter (see the left bottom panel of the figure). For 'narrow' pulses, the spectrum is always harder than that of the emission expected from the tip of fireball, and the deviation is obvious and it is very significant in the decaying portion of the light curve.

In the case of the soft-to-hard-to-soft intrinsic spectrum, the observed spectra in the rising part of the light curve are softer than, but quite close to, that expected from the emission of the tip of fireball. In the decaying phase, they are much harder than the latter for 'narrow' pulses and are almost the same as the latter for 'broad' pulses.

3.3.2. Peak energy

One might notice that the magnitude of the spectrum of the emission expected to originate from the tip of fireball discussed above is not real since the emission from other parts of the fireball is much larger than that merely from the tip and hence they are not comparable. However, the concept of this spectrum is useful since it does represent the real form of emission from the tip. After all, it is the form that determines how 'hard' a spectrum is.

Now we turn our attention to investigating how large the deviation is of the spectrum arising from the whole fireball surface from that of the emission of the tip of fireballs in terms of the peak energy. We define the deviation of the peak energy of the spectrum of the whole fireball emission from that of the tip as

$$\Delta E_{\rm p} \equiv E_{\rm p} - E_{\rm p,tip}, \tag{54}$$

where $E_{\rm p,tip}$ is the peak energy of the spectrum of the emission expected to originate from the tip.

Displayed in Fig.8 are the relations between $\Delta E_{\rm p}$ and time derived from various cases. Conclusions obtained above are reinforced. a) In the case of the unchanged intrinsic spectrum, the spectrum arising from the whole fireball surface is always softer than the spectrum coming merely from the tip (see also Fig.5). In the decaying phase of the pulses, the softening becomes stronger and stronger. b) When the intrinsic spectrum evolves in the way to follow a simple hard-to-soft pattern, the spectrum originating from the whole fireball surface is always harder than that

coming merely from the tip (which is beyond our initial expectation) (see also Fig.6). c) For a soft-to-hard-to-soft spectral evolution, the spectrum of the whole fireball surface becomes softer than that from the tip during the rising phase of the pulses, and then turns harder than the latter in the decaying phase (see also Fig.7). d) For 'broad' pulses, the hardening in the decaying phase in the latter two cases is very mild and thus the observed spectrum could serve as a good estimator of that from the tip emission. e) In the case of 'narrow' pulses, the hardening in the decaying phase is so strong that one cannot estimate the intrinsic spectrum from an observed one. A consequence of this phenomenon is that in the decaying phase, 'narrow' pulses are generally harder than 'broad' ones. This could possibly be checked by current observations.

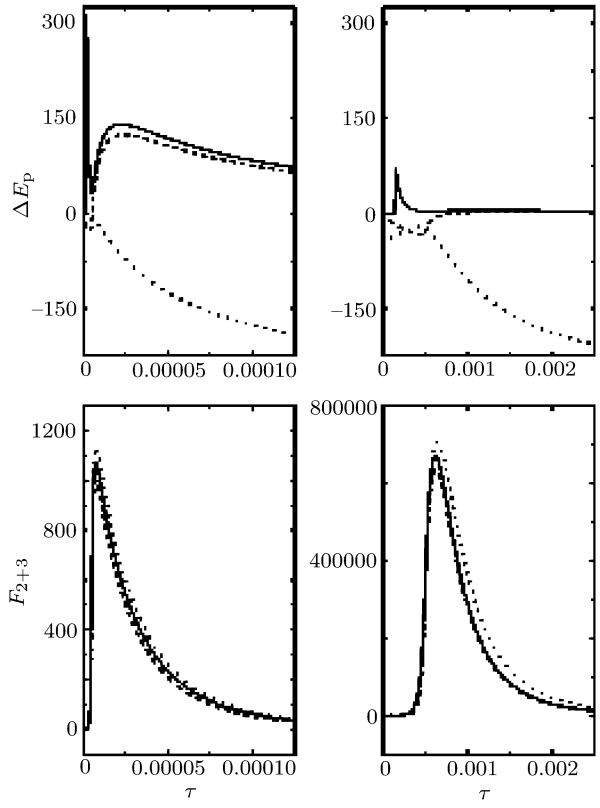


Fig.8. Evolutions of $\Delta E_{\rm p}$ (upper panels) for 'narrow' (left panels) and 'broad' (right panels) pulses, calculated from expression (54). Light curves of the integrated flux F_{2+3} (in the bottom panels) are also presented (see Fig.4) for a direct comparison. Parameters and symbols are the same as those in Fig.4.

One might notice that the deviation of the peak energy is sensitive in the rising part of pulses. In the case of the simple hard-to-soft intrinsic spectral evolution pattern, the observed peak energy could become about 300 keV larger than that expected from the tip of fireballs when the pulses observed are relatively narrow, and it could be about 70 keV larger than that of the tip when the pulses concerned are relatively broad. In the decaying phase, $E_{\rm p}$ could be about 50–150 keV larger than that of the tip for 'narrow' pulses whilst it is almost the same as that of the tip for 'broad' ones.

3.4. Spectral evolution revealed in other aspects

3.4.1. Relation between flux and peak energy

An important aspect capable of revealing spectral evolution in GRB pulses is a well-known relation between flux and peak energy. From Fig.2 of Ref.[29], the observed flux F was found to be significantly correlated with the peak energy $E_{\rm p}$ within a single burst for a subset of their samples. In their study, F was the integrated flux in a wide energy range which was also adopted in Ref.[30]. Here we explore the relation between the integrated flux and peak energy expected to be emitted from a fireball pulse. Several cases discussed above are studied on this issue.

The results are shown in Fig.9, where the adopted energy range confining the integrated flux is 1–10000 keV. A linear relation between the two quantities in logarithm, i.e. $\log F/F_{\rm max}$ and $\log E_{\rm p}$, is seen in the decaying phase of pulses. In terms of statistics, the relation is called the hardness-intensity correlation (HIC) which was noticed by many authors engaged in gamma-ray bursts.[24,28,29,31,32] There is a turnover feature in the relation between the two quantities. The turnover feature leads to a hook-like curve which is sensitive to intrinsic spectral evolution patterns. An intrinsic soft-to-hard-to-soft spectral evolution corresponds to a semi-linear correlation between $\log F$ and $\log E_{\rm p}$ in the rising phase of pulses, with its slope being larger than that in the decaying phase. In the case of an unchanged intrinsic spectrum, the relation in the rising phase is a straight line parallel to the F axis. When the intrinsic spectral evolution pattern is a simple hard-to-soft one, the observed integrated flux F would decrease with the increase of $E_{\rm p}$ in the rising phase.

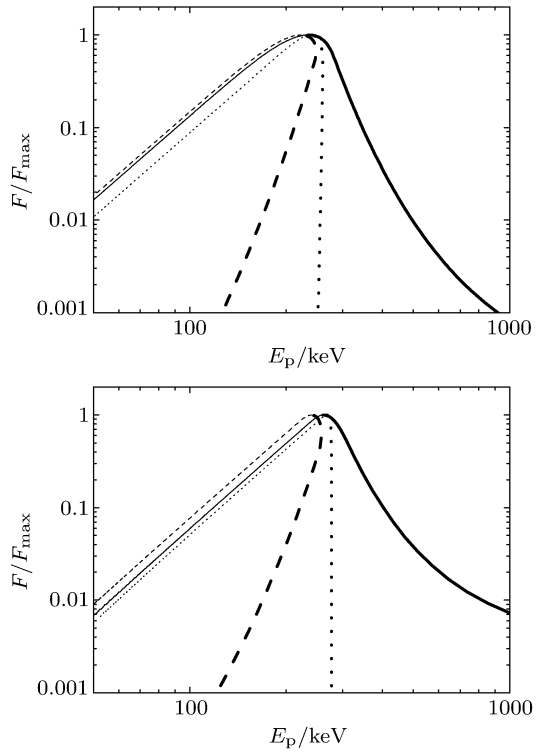


Fig.9. Relations between integrated flux and peak energy in the cases of unchanged intrinsic spectrum (dotted lines), hard-to-soft intrinsic spectrum (solid lines), and soft-to-hard-to-soft intrinsic spectrum (dashed lines) for 'narrow' (in the bottom panel) and 'broad' (in the upper panel) pulses of fireball, where thin lines denote the relation in the decaying phase of pulses and thick lines represent that in the rising part of the light curve of pulses.

Relations between the integrated flux and the peak energy in the decaying phase of all the six pulses discussed above are calculated. They are found to strictly follow a power law: $F \propto E_{\rm p}^{\gamma}$, with $\gamma \approx 3$. This is in agreement with what was found in Ref.[16] in a recent investigation.

3.4.2. Relevant relations

The first relevant relation discussed here is the relation between the peak value of the νf_ν spectrum and the peak energy $E_{\rm p}$, which was previously investigated in Ref.[28]. We study all the six pulses discussed above and find that the relation is similar to that between the flux and the peak energy (the figure is very similar to Fig.9, and so it is omitted here). We find the same power law relation $(\nu f_\nu)_{\rm p} \propto E_{\rm p}^{\gamma}$ in the decaying phase of pulses and approximately the same index $\gamma \approx 3$.

The second relation is the relation between the flux f_ν at a fixed energy E and the spectral peak energy $E_{\rm p}$. Here we adopt E=200 keV. All the six pulses discussed above are studied. Apart from a slight difference, the relation is similar to that between the flux and the peak energy (the figure is omitted here). Although f_ν increases with the increase of $E_{\rm p}$ in the decaying phase of pulses, the relation is no more of a power law.

The third relation is the relation between the integrated flux over the energy range adopted above (see Fig.9) and the hardness ratio. The hardness ratio adopted here is defined as EHR$\equiv F_3/F_2$, where F_2 and F_3 are the integrated fluxes confined in the energy ranges of the second and third BATSE channels, respectively. Shown in Fig.10 is the relation in various cases discussed in Fig.9. In the decaying phase of the six pulses concerned, the relation is not of a power law, but still, the integrated flux increases with hardness ratio increasing.

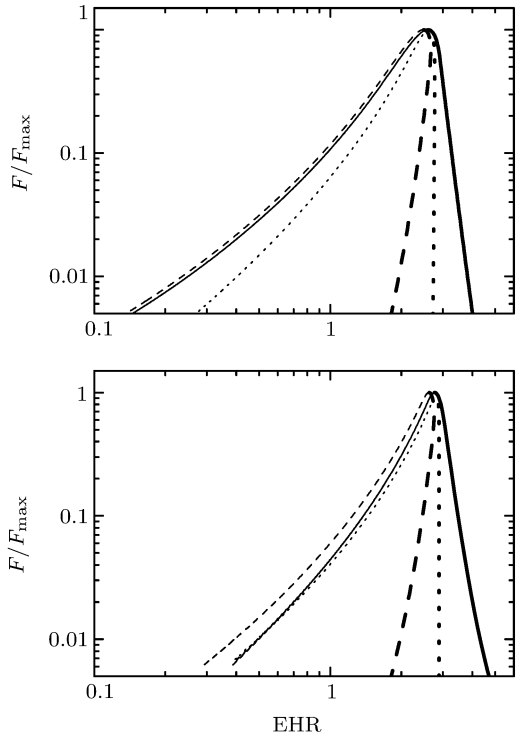


Fig.10. Relations between the integrated flux and the hardness ratio. The symbols are the same as those in Fig.9.

4. Spectral evolution of pulses associated with other intrinsic emission forms

The real GRB emission might be more complicated than what was discussed above. We wonder whether different intrinsic emission forms could lead to other conclusions.

Following Ref.[16], we adopt an intrinsic broken-power-law (BPL) spectrum in the emission of a pulse.

This pulse is assumed to possess a linear rise and a linear decay. In the same way we consider three evolutionary patterns which are unchanged, hard-to-soft, and soft-to-hard-to-soft respectively.

The co-moving pulse is assumed to be

$$\tilde{I}_{0,\nu}(\tau_0,\nu_0) = I_0 \left\{ \begin{array}{l} \left(\dfrac{\nu_0}{\nu_{0,\mathrm{b}}}\right)^{1+\alpha}, \ (\nu_0 \le \nu_{0,\mathrm{b}}), \\ \left(\dfrac{\nu_0}{\nu_{0,\mathrm{b}}}\right)^{1+\beta}, \ (\nu_{0,\mathrm{b}} < \nu_0), \end{array} \right\} \left\{ \begin{array}{l} \dfrac{\tau_0 - \tau_{0,\min}}{\tau_{0,0} - \tau_{0,\min}}, \ (\tau_{0,\min} < \tau_0 \le \tau_{0,0}), \\ \dfrac{\tau_{0,\max} - \tau_0}{\tau_{0,\max} - \tau_{0,0}}, \ (\tau_{0,0} < \tau_0 < \tau_{0,\max}), \end{array} \right. \tag{55}$$

where $\nu_{0,\mathrm{b}}$ is a function of τ_0. Co-moving pulse (55) is a pulse with a linear rise and a linear decay, emitting in a BPL radiation form. In the case of an unchanged intrinsic spectrum, $\nu_{0,\mathrm{b}}$ is taken as $\nu_{0,\mathrm{b}} = \nu_{0,0}$ when $\tau_{0,\min} < \tau_0 < \tau_{0,\max}$ (where $\nu_{0,0}$ is a constant). In the case of a hard-to-soft intrinsic spectrum, $\nu_{0,\mathrm{b}}$ is assumed to decrease linearly with the increase of τ_0, i.e. $\nu_{0,\mathrm{b}} = \dfrac{\tau_{0,0} - \tau_{0,\min}}{\tau_0 - \tau_{0,\min}}\nu_{0,0}$ when $\tau_{0,\min} < \tau_0 < \tau_{0,\max}$. In the case of a soft-to-hard-to-soft intrinsic spectrum, $\nu_{0,\mathrm{b}}$ is assumed to rise linearly and then drop also linearly with the increase of τ_0, i.e. $\nu_{0,\mathrm{b}} = \dfrac{\tau_0 - \tau_{0,\min}}{\tau_{0,0} - \tau_{0,\min}}\nu_{0,0}$ when $\tau_{0,\min} < \tau_0 \le \tau_{0,0}$, and $\nu_{0,\mathrm{b}} = \dfrac{\tau_{0,\max} - \tau_0}{\tau_{0,\max} - \tau_{0,0}}\nu_{0,0}$ when $\tau_{0,0} < \tau_0 < \tau_{0,\max}$.

One might notice that the broken-power-law model could well approximate the band function model[33] in very low and high energy ranges. We accordingly assign the typical values of the low and the high energy indices available from the fit of the Band function model to BATSE GRB spectra to be the corresponding values for the BPL model used here, i.e. $\alpha = -1$ and $\beta = -2.25$.[34,35] In addition, we assign $\tau_{0,\min} = 0$ and take $\tau_{0,\max} - \tau_{0,0} = 2(\tau_{0,0} - \tau_{0,\min})$. We take $\Gamma = 100$ so that a direct comparison with those results in Section 3 could be made.

We study the evolutionary curve of the peak energy (EPC) for the case of the broken-power-law-type emission (55) emitted in unchanged, hard-to-soft, and soft-to-hard-to-soft intrinsic spectra for 'narrow' and 'broad' pulses of fireball (the half width in the rising phase of the 'narrow' co-moving pulse is taken as 0.0001, and that of the 'broad' one is 0.01). The analysis shows that the conclusions drawn from Fig.4 hold in this situation (the relevant figure is omitted). Noticeable differences are as follows: in the case of 'narrow' pulses, the EPC arising from the hard-to-soft intrinsic spectrum is significantly larger than that stemming from the unchanged and soft-to-hard-to-soft intrinsic spectra in the decaying phase; in the case of 'broad' pulses, the EPC arising from the unchanged intrinsic spectrum is larger than that originating from the other two intrinsic spectra in the decaying phase and it seems to deviate from the common trend observed in other cases.

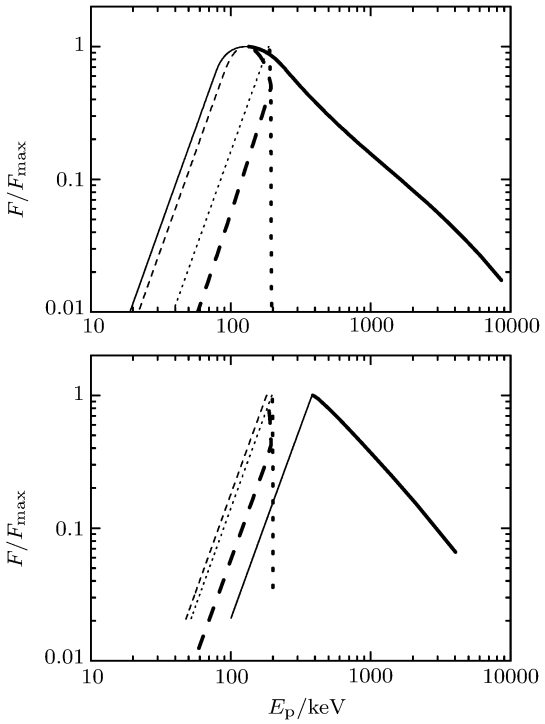


Fig.11. Relations between integrated flux and peak energy in the case of the broken-power-law-type emission (55) with unchanged intrinsic spectrum (dotted lines), hard-to-soft intrinsic spectrum (solid lines), and soft-to-hard-to-soft intrinsic spectrum (dashed lines) for 'narrow' (in the bottom panel) and 'broad' (in the upper panel) pulses of fireballs. Parameters and their relation are $\alpha = -1$, $\beta = -2.25$, $\tau_{0,\min} = 0$, $\Gamma = 100$, and $\tau_{0,\max} - \tau_{0,0} = 2(\tau_{0,0} - \tau_{0,\min})$ respectively. The half width in the rising phase of the 'narrow' co-moving pulse is taken as 0.0001, and that of the 'broad' one is 0.01. The thick and thin lines denote what their counterparts represent in Fig.9.

Relations between integrated flux and peak energy for the three intrinsic pulses confined by the three $\nu_{0,\rm b}(\tau_0)$ functions mentioned above are shown in Fig.11. The turnover features shown in Fig.9 are also observed in this figure. The power law relation between the two quantities in the decaying phase of pulses holds for all cases concerned here, where the index is found to be $\gamma \approx 3$ as well. In addition, we notice that the whole curves of the F–$E_{\rm p}$ relation vary significantly with the intrinsic emission, and the range of the power law relation depends strongly on the emission as well.

5. Spectral evolution of pulses expected in other situations of the soft-to-hard-to-soft intrinsic emission

In the analysis of the soft-to-hard-to-soft intrinsic emission of co-moving pulses performed above, the peak energy of the intrinsic emission concerned is that starting from and ending at very low energy and the hardest intrinsic spectrum occurs at the time when the peak flux of the co-moving pulse appears. This might not be true in practice. In fact, a co-moving pulse might start to emit in a high energy region and then reaches the maximum and then drops to the minimum which still remains in a high energy region. In particular, some pulses might arise from the emission in which the hardest intrinsic spectrum appears ahead of the peak flux. We are anxious to know whether the conclusions obtained above are affected due to all that is taken into account.

Two co-moving pulses with a skew soft-to-hard-to-soft spectrum, starting to emit in a high energy region and ending its emission in a relatively low energy region are considered. One is a modified Comptonized radiation form (52) as follows:

$$\tilde{I}_{0,\nu}(\tau_0,\nu_0) = I_0\nu_0^{1+\alpha_C}\begin{cases} 0, & (\tau_{0,\min} < \tau_0 \le \tau_{0,1}),\\ \exp[-(\tau_{0,p}/\tau_0)(\nu_0/\nu_{0,\rm C})]\exp\left(-\dfrac{\tau_{0,0}-\tau_0}{\sigma_{\rm r}}\right), & (\tau_{0,1} < \tau_0 \le \tau_{0,p}),\\ \exp[-(\tau_0/\tau_{0,p})(\nu_0/\nu_{0,\rm C})]\exp\left(-\dfrac{\tau_{0,0}-\tau_0}{\sigma_{\rm r}}\right), & (\tau_{0,p} < \tau_0 \le \tau_{0,0}),\\ \exp[-(\tau_0/\tau_{0,p})(\nu_0/\nu_{0,\rm C})]\exp\left(-\dfrac{\tau_0-\tau_{0,0}}{\sigma_{\rm d}}\right), & (\tau_{0,0} < \tau_0 \le \tau_{0,2}), \end{cases} \tag{56}$$

where $\tau_{0,p} = \tau_{0,0} - \Delta\tau_0$ and $\Delta\tau_0$ represents the time interval for the hardest spectrum to appear ahead of the time the peak flux occurs. We assign $\tau_{0,1} = \tau_{0,p}/2$ and $\tau_{0,2} = 2\tau_{0,p}$. In applying co-moving pulse (56), we take $\Delta\tau_0 = \sigma_{\rm r}$, $\sigma_{\rm r} = 0.01$ and $\Gamma = 100$, and adopt all other parameters the same as those adopted in Section 3 (see the caption of Fig.1).

The other is a revised broken-power-law-type emission form which is still described by expression (55), with $\nu_{0,\rm b}$ determined by $\nu_{0,\rm b} = \dfrac{\tau_0 + \tau_{0,p} - 2\tau_{0,\min}}{2(\tau_{0,p} - \tau_{0,\min})}\nu_{0,0}$ when $\tau_{0,\min} < \tau_0 \le \tau_{0,p}$ and $\nu_{0,\rm b} = \dfrac{2\tau_{0,\max} - \tau_{0,p} - \tau_0}{2(\tau_{0,\max} - \tau_{0,p})}\nu_{0,0}$ when $\tau_{0,p} < \tau_0 < \tau_{0,\max}$ (where $\tau_{0,p} = \tau_{0,0} - \Delta\tau_0$). In applying co-moving pulse (55) together with this relation, we assign $\tau_{0,\min} = 0$ and take $\tau_{0,\max} - \tau_{0,0} = 2(\tau_{0,0} - \tau_{0,\min})$, $\alpha = -1$, $\beta = -2.25$, and $\Gamma = 100$, as adopted in the last section. We consider only a 'broad' co-moving pulse and therefore take its half width in the rising phase as 0.01.

For these two co-moving pulses, we explore the peak energy evolutionary curve and the relation between integrated flux and energy. They are shown in Figs.12 and 13 respectively. Figure 12 shows that the skewness leads to a forward shift of the peak of EPC. It makes the offset of the peak of EPC larger (see Fig.4). The EPC in the decaying phase is obviously less affected by the factors considered here. It is interesting that the shape of the EPC is the shape of an incomplete pulse. The lack of the very small values of $E_{\rm p}$ in the rising phase must be due to the fact that the co-moving pulses are assumed to start to

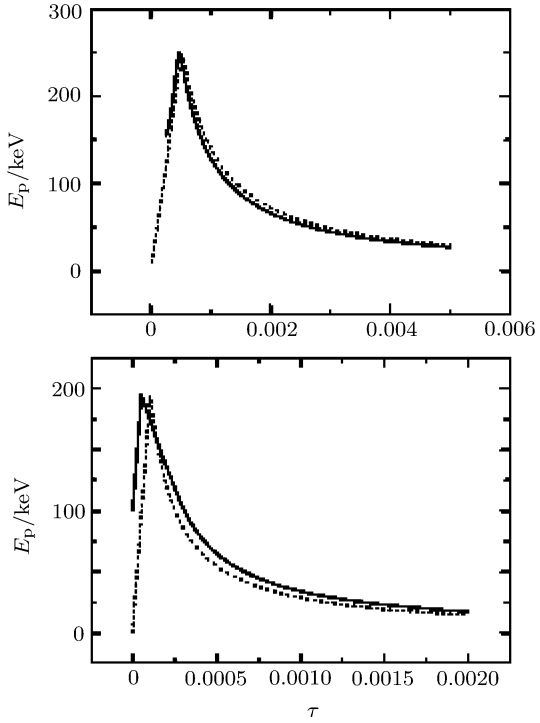


Fig.12. Evolutionary curves of the peak energy associated with co-moving pulses with a skew soft-to-hard-to-soft spectrum. In the upper panel, the solid line is the curve arising from co-moving pulse (56); the dotted line is the dashed line in the upper left panel of Fig.4. In the bottom panel, the solid line is the curve arising from co-moving pulse (55) coupling the $\nu_{0,\mathrm{b}}(\tau_0)$ function presented in Section 5; the dotted line is the curve arising from co-moving pulse (55) coupling the soft-to-hard-to-soft $\nu_{0,\mathrm{b}}(\tau_0)$ function presented in Section 4. The pulses concerned are 'broad' ones (see Section 5 for the details of the adopted parameters).

emit at a high energy region. This assumption seems to be reasonable, and therefore one could expect the EPC of GRB pulses to possess an incomplete pulse shape if these pulses suffer from the curvature effect. As shown in the EPC, the power law relation between flux and peak energy in the decaying phase is stubborn (see Fig.13). The factors concerned have no influence on this relation. On the contrary, the relation in the rising phase changes significantly according to the evolutionary pattern of intrinsic emission. As shown in Fig.13, although the curves in the rising phase are so different, they are all on the right-hand-side of the decaying curve, which makes the relation within the whole pulse interval a hook-like curve.

As proposed in Section 3, it will be natural that a co-moving pulse experiences a soft-to-hard spectral evolution phase (which might be quite short) and then a hard-to-soft phase during a shock. One thus can expect that the features of the curves studied in this section might be common in the GRB pulses if they do arise from the emission of a relativistically expanding fireball.

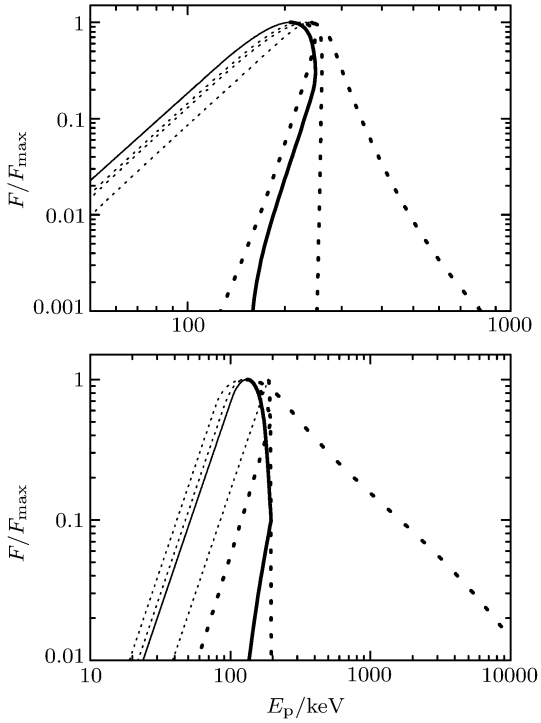


Fig.13. Relation between the integrated flux and peak energy associated with co-moving pulses with a skew soft-to-hard-to-soft spectrum. In the upper panel, the solid line denotes the curve arising from co-moving pulse (56), and the dotted lines represent all the lines in the upper panel of Fig.9. In the bottom panel, the solid line refers to the curve arising from co-moving pulse (55) coupling with the $\nu_{0,\mathrm{b}}(\tau_0)$ function presented in Section 5, and the dotted lines denote all the lines in the upper panel of Fig.11. Parameters are the same as those in Fig.12. The thin solid line represents the decaying phase of pulses and the thick solid line denotes the rising phase.

6. Influence of the Lorentz factor

In the above analysis, one important factor, the Lorentz factor of the expanding motion of fireballs, was not taken into account. Would it give rise to entirely different results, if it is taken into account? We explore this issue by adopting various values of the Lorentz factor and then comparing the results. The peak energy evolutionary curve and the relation between the integrated flux and peak energy are investigated.

We adopt the intrinsic pulses discussed in the previous section to study this issue, where parameters other than the Lorentz factor remain unchanged. The Lorentz factor $\Gamma = 100$ is replaced with $\Gamma = 10$ and

$\Gamma = 1000$ separately to show whether this quantity plays a role in the two relationships concerned. The analysis shows that although the adopted Lorentz factors are significantly different, the features of EPC observed in Fig.12 are unchanged (the figure is omitted). Shown in Fig.14 are the relations between the integrated flux and peak energy, calculated with the two Lorentz factors. The shapes of the curves for the integrated flux versus peak energy are the same as those shown in Fig.13. The index of the power law relation between the integrated flux and peak energy in the decaying phase changes a little. In the case of the revised broken-power-law-type emission, the index (γ) ranges from 2.84 (for $\Gamma = 10$) to 2.99 (for $\Gamma = 1000$); and in the case of the modified Comptonized radiation, the index (γ) changes from 2.95 (for $\Gamma = 10$) to 3.07 (for $\Gamma = 1000$). It seems that the larger the Lorentz factor is, the larger the value of index will be. A noticeable feature revealed in Fig.14 is the shift of the peak energy range, which is expected due to the Doppler shifting.

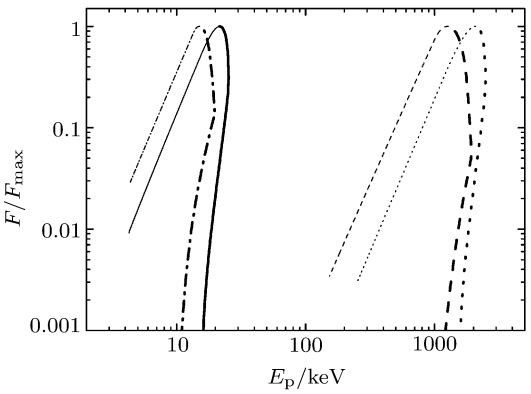


Fig.14. Relations between the integrated flux and peak energy arising from fireballs expanding with $\Gamma = 10$ (the solid line and the dashed dotted line respectively) and $\Gamma = 1000$ (the dashed line and the dotted line respectively) separately. The dashed dotted line and the dashed line denote the curves associated with the revised broken-power-law-type emission and the co-moving pulse (55) coupling with the $\nu_{0,\rm b}(\tau_0)$ function presented in Section 5, respectively; the solid line and the dotted line represent the curves associated with the modified Comptonized radiation and the co-moving pulse (56), respectively. Parameters other than the Lorentz factor are the same as those adopted in Fig. 13. Thin lines refer to the decaying phase of pulses and thick lines denote the rising phase.

7. Symbol of the curvature effect

It is known that light curves arising from the emission of an intrinsic δ-function pulse with a monochromatic radiation over the whole fireball surface share the same profile, a marginal decaying curve.[17] Light curves of real emission are found to deviate from this curve by a reverse-S feature in their decaying phase and this could serve as a symbol of the curvature effect. Here we consider a co-moving δ-function pulse radiated at a fixed energy (a mono-colour radiation), trying to find whether there exists a similar curve in terms of the peak energy.

The co-moving δ-function pulse with a monochromatic radiation is taken as

$$\tilde{I}_{0,\nu}(\tau_0,\nu_0) = I_0\delta(\tau_0-\tau_{0,0})\delta(\nu_0-\nu_{0,0}), \quad (0\le\tau_{0,0}). \tag{57}$$

Without any loss of generality, we take $\tau_{0,0} = 0$. When applying inequality (40) we take $\tau_{0,\min} = \tau_{0,\max} = 0$ since τ_0 is confined by $\tau_{0,\min} \le \tau_0 \le \tau_{0,\max}$ and there is emission only at $\tau_0 = \tau_{0,0} = 0$. We consider the emission from the whole fireball surface and then take $\theta_{\min} = 0$ and $\theta_{\max} = \pi/2$. Thus, from inequality (40) we obtain inequality $0 \le \tau \le 1$. The relation between the observed frequency and the emitted rest frame frequency is expressed as formula (36). Applying expression (57), the formula turns into

$$\nu(\tau) = \frac{\nu_{0,0}}{(1-\beta+\beta\tau)\Gamma}, \tag{58}$$

which describes the development of ν that arises from the emission of a co-moving δ-function pulse radiated with a monochromatic spectrum.

One can check that the maximum of ν is reached when $\tau = 0$. The maximum of ν is expressed as $\nu_{\max} = \dfrac{\nu_{0,0}}{(1-\beta)\Gamma}$. Expression (58) then could be written as $\dfrac{\nu(\tau)}{\nu_{\max}} = \dfrac{1-\beta}{1-\beta+\beta\tau}$. Taking $\nu/\nu_{\max} = 1/2$ yields $\tau_{\rm h} = \dfrac{1-\beta}{\beta}$, which denotes the time when the observed frequency is half the maximum of ν. Combining these relations we obtain

$$\frac{\nu(\tau)}{\nu_{\max}} = \frac{1}{1+\tau/\tau_{\rm h}}, \tag{59}$$

which shows that in terms of $\tau/\tau_{\rm h}$, the curve $\nu/\nu_{\max}$ is independent of the Lorentz factor.

Now we study various $E_{\rm p}(t)$ curves discussed above in terms of $t'/t'_{\rm h}$, where t' is the observation time set to the moment when the maximum of $E_{\rm p}$, $E_{p,\max}$, is observed, and $t'_{\rm h}$ denotes the time t' when the observed $E_{\rm p}$ is half the value of $E_{p,\max}$. [Note that $t'/t'_{\rm h} = \tau/\tau_{\rm h}$ since the coefficient relating t' to τ

is cancelled; see expression (35).] As shown in Fig.4, the spectral behaviour in terms of $E_{\rm p}$ in the decaying phase of fireball pulses is quite stubborn. This is due to the fact that the curvature effect dominates the evolution of the observed spectrum in this period. We thus examine how other evolutionary curves of the peak energy in this period differ from the curve of (59) which we call the marginal decaying form of the peak energy evolutionary curve.

We compare the $E_{\rm p}(t)$ curves in the decaying phase of the six pulses discussed in Section 3 (see the caption of Fig.2) with the curve of (59) and find that the former well follows the latter, where only very minute deviations are observed (the figure is omitted here). It is interesting that when a deviation is perceivable, the $E_{\rm p}(t)$ evolutionary curve must possess a reverse-S feature relative to the curve of (59). The result indicates that the marginal decaying form (59) could serve as a symbol of the curvature effect.

Do these conclusions hold in the cases of other intrinsic emission forms and other values of the Lorentz factor discussed above in Sections 4–6? The answer is yes. Presented in Fig.15 is the peak energy evolutionary curve arising from a 'broad' co-moving pulse of the broken-power-law-type emission (55) with an unchanged intrinsic spectrum in the decaying phase of the pulse, which is seen to possess the most deviation from the marginal decaying curve (59), detected from the peak energy evolutionary curves of all the situations discussed above. We find that the conclusions are not violated by all these factors.

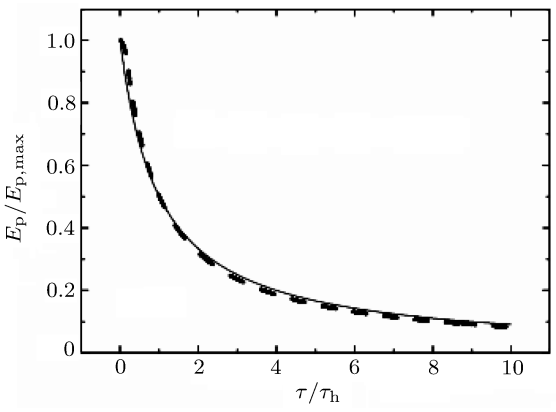


Fig.15. Evolutionary curve (the dashed line) of the peak energy $E_{\rm p}$ in the decaying phase of a 'broad' fireball pulse in the case of the broken-power-law-type emission (55) with an unchanged intrinsic spectrum (see the caption of Fig.11). The solid line is the curve of (59).

8. Conclusions

It is known that the power indices in the relation between flux and peak energy derived from many GRBs are different from those expected by the curvature effect. Some possible interpretations for this variation were proposed in Ref.[16]: adiabatic and radiative cooling processes that extend the decay timescale, a nonuniform jet, and the formation of pulses by external shock processes. According to our analysis, the first one seems unlikely. The cooling time, long or short, is in fact included in the decaying phase of co-moving pulses, and the decaying portion of the pulses has little influence on the power index. Authors of Ref.[15] proposed that the breaking of local spherical symmetry such as a prolate or oblate shell geometry would cause the power law index to be different from that in the spherical case. This interpretation is somewhat similar to that from the second proposal of Ref.[16] and might be an interesting outlet for the problem. In an investigation on the hardness-intensity correlation (HIC) in GRB pulses, authors of Ref.[28] found that some pulses exhibited a track jump in their HICs, in which the correlation jumps between two power laws with the same index. This was interpreted as a symbol of the existence of strongly overlapping pulses. This mechanism would naturally explain why the index observed in some GRBs could be larger or smaller than predicted by the curvature effect. For example, an upper power law line in Fig.9 jumping to a lower power law line in the figure would give rise to a smaller index, while a lower line jumping to an upper line would produce a larger index.

In the relation between the integrated flux and the peak energy, the following conclusions hold: in the decaying phase of pulses, the two quantities are well related by a power law with the index being about 3, which is irrelative to the intrinsic emission and the Lorentz factor; the relation in the rising phase can be different for different pulses significantly and the overall relation between the two quantities varies and shifts enormously, depending on the form or width of the intrinsic emission of pulse and on parameters such as the Lorentz factor.

The pattern of the spectral evolution of the intrinsic emission of a co-moving pulse within its rising phase could be observed in the relation between the integrated flux and peak energy. For an unchanged intrinsic spectrum, the relation in the rising phase is a straight line in parallel to the axis of the flux; for

a hard-to-soft intrinsic spectrum, the flux decreases with the increase of the peak energy within this phase; for a soft-to-hard-to-soft intrinsic spectrum, the flux generally increases with the increase of the peak energy in the rising phase.

Besides the above conclusions, the following conclusions could also be reached for pulses arising from a relativistically expanding fireball. a) The spectra of a pulse in its decaying phase differ slightly for different intrinsic spectral evolution patterns, and hence the curvature effect must play a predominant role. b) An intrinsic soft-to-hard-to-soft spectral evolution within a co-moving pulse would give rise to a pulse-like evolutionary curve for the peak energy. c) There exists a marginal form of $1/(1+\tau/\tau_{\rm h})$ for the peak energy evolutionary curve in the decaying phase of pulses, and in many cases the peak energy evolutionary curve well follows the form and when the former deviates from the latter it deviates in a reverse-S way.

References

[1] Rees M J and Meszaros P 1994 *Astrophys. J.* **430** L93

[2] Burrows D N, Romano P, Falcone A, Kobayashi S, Zhang B, Moretti A, O'Brien P T, Goad M R, Campana S, Page K L, Angelini L, Barthelmy S, Beardmore A P, Capalbi M, Chincarini G, Cummings J, Cusumano G, Fox D, Giommi P, Hill J E, Kennea J A, Krimm H, Mangano V, Marshall F, Mészáros P, Morris D C, Nousek J A, Osborne J P, Pagani C, Perri M, Tagliaferri G, Wells A A, Woosley S and Gehrels N 2005 *Science* **309** 1833

[3] Tagliaferri G, Goad M, Chincarini G, Moretti A, Campana S, Burrows D N, Perri M, Barthelmy S D, Gehrels N, Krimm H, Sakamoto T, Kumar P, Mészáros P I, Kobayashi S, Zhang B, Angelini L, Banat P, Beardmore A P, Capalbi M, Covino S, Cusumano G, Giommi P, Godet O, Hill J E, Kennea J A, Mangano V, Morris D C, Nousek J A, O'Brien P T, Osborne J P, Pagani C, Page K L, Romano P, Stella L and Wells A 2005 *Nature* **436** 985

[4] Butler N R and Kocevski D 2007 *Astrophys. J.* **663** 407

[5] Nousek J A, Kouveliotou C, Grupe D, Page K L, Granot J, Ramirez-Ruiz E, Patel S K, Burrows D N, Mangano V, Barthelmy S, Beardmore A P, Campana S, Capalbi M, Chincarini G, Cusumano G, Falcone A D, Gehrels N, Giommi P, Goad M R, Godet O, Hurkett C P, Kennea J A, Moretti A, O'Brien P T, Osborne J P, Romano P, Tagliaferri G and Wells A A 2006 *Astrophys. J.* **642** 389

[6] O'Brien P T, Willingale R, Osborne J, Goad M R, Page K L, Vaughan S, Rol E, Beardmore A, Godet O, Hurkett C P, Wells A, Zhang B, Kobayashi S, Burrows D N, Nousek J A, Kennea J A, Falcone A, Grupe D, Gehrels N, Barthelmy S, Cannizzo J, Cummings J, Hill J E, Krimm H, Chincarini G, Tagliaferri G, Campana S, Moretti A, Giommi P, Perri M, Mangano V and LaParola V 2006 *Astrophys. J.* **647** 1213

[7] Zhang B, Fan Y Z, Dyks J, Kobayashi S, Mészáros P, Burrows D N, Nousek, J A and Gehrels N 2006 *Astrophys. J.* **642** 354

[8] Zhang B B, Liang E W and Zhang B 2007 *Astrophys. J.* **666** 1002

[9] Qin Y P, Su C Y, Fan J H and Gupta A C 2006 *Phys. Rev.* D **74** 063005

[10] Fenimore E E, Madras C D and Nayakshin S 1996 *Astrophys. J.* **473** 998

[11] Sari P and Piran T 1997 *Astrophys. J.* **485** 270

[12] Kumar P and Panaitescu A 2000 *Astrophys. J.* **541** L51

[13] Qin Y P 2002 *Astro. Astrophys.* **396** 705

[14] Ryde F and Petrosian V 2002 *Astrophys. J.* **578** 290

[15] Kocevski D, Ryde F and Liang E 2003 *Astrophys. J.* **596** 389

[16] Dermer C D 2004 *Astrophys. J.* **614** 284

[17] Qin Y P and Lu R J 2005 *Mon. Not. Roy. Astron. Soc.* **362** 1085

[18] Shen R F, Song L M and Li Z 2005 *Mon. Not. Roy. Astron. Soc.* **362** 59

[19] Qin Y P, Zhang Z B, Zhang F W and Cui X H 2004 *Astrophys. J.* **617** 439

[20] Qin Y P, Dong Y M, Lu R J, Zhang B B and Jia L W 2005 *Astrophys. J.* **632** 1008

[21] Zhang F W and Qin Y P 2005 *Chin. Phys.* **14** 2276

[22] Liang E W, Zhang B, O'Brien P T, Willingale R, Angelini L, Burrows D N, Campana S, Chincarini G, Falcone A, Gehrels N, Goad M R, Grupe D, Kobayashi S, Mészáros P, Nousek J A, Osborne J P, Page K L and Tagliaferri G 2006 *Astrophys. J.* **646** 351

[23] Lu R J, Qin Y P and Zhang F W 2007 *Chin. Phys.* **16** 1806

[24] Norris J P, Share G H, Messina D C, Dennis B R, Desai U D, Cline T L, Matz S M and Chupp E L 1986 *Astrophys. J.* **301** 213

[25] Kargatis V E, Liang E P and BATSE Team 1995 *Astrophys. Space Sci.* **231** 177

[26] Ryde F and Svensson R 2000 *Astrophys. J.* **529** L13

[27] Ryde F and Svensson R 2002 *Astrophys. J.* **566** 210

[28] Borgonovo L and Ryde F 2001 *Astrophys. J.* **548** 770

[29] Liang E W, Dai Z G and Wu X F 2004 *Astrophys. J.* **606** L29

[30] Yonetoku D, Murakami T, Nakamura T, Yamazaki R, Inoue A K and Ioka K 2004 *Astrophys. J.* **609** 935

[31] Kargatis V E, Liang E P, Hurley K C, Barat C, Eveno E and Niel M 1994 *Astrophys. J.* **422** 260

[32] Band D 1997 *Astrophys. J.* **486** 928

[33] Band D, Matteson J, Ford L, Schaefer B, Palmer D, Teegarden B, Cline T, Briggs M, Paciesas W, Pendleton G, Fishman G, Kouveliotou C, Meegan C, Wilson R and Lestrade P 1993 *Astrophys. J.* **413** 281

[34] Preece R D, Pendleton G N, Briggs M S, Mallozzi R S, Paciesas W S, Band D L, Matteson J L and Meegan C A 1998 *Astrophys. J.* **496** 849

[35] Preece R D, Briggs M S, Mallozzi R S, Pendleton G N, Paciesas W S and Band D L 2000 *Astrophys. J. Suppl.* **126** 19